

Far-Ultraviolet Reflectance Spectra and the Electronic Structure of Ionic Crystals*

G. W. Rubloff^{†‡§}

Department of Physics, The University of Chicago, Chicago, Illinois 60637

(Received 17 September 1971)

The use of synchrotron radiation as a light source has made possible the measurement of the normal-incidence reflectance spectra of a number of ionic crystals in the photon energy range $6 \text{ eV} < \hbar\omega < 36 \text{ eV}$ for temperatures $90^\circ\text{K} < T < 400^\circ\text{K}$. The crystals investigated include KCl, KBr, RbCl, CsCl, CsBr, CaF_2 , SrF_2 , and BaF_2 . The spectra are compared and analyzed with particular reference to their dependence on temperature, chemical composition, and crystal structure. Special attention is given to the region of the spectra dominated by electronic excitation of the p core levels which form the outer shell of the $+$ ions. Sharp peaks (width $\leq 0.2 \text{ eV}$) characterize the lower-energy portion of this region. They are correlated with the identity of the $+$ ion and are assigned to transitions in the Brillouin zone using their observed temperature dependence and separation. The evidence is analyzed and found to favor the interpretation of these peaks as core excitons. At higher energies, there appear broader structures (width $> 0.5 \text{ eV}$) considered to be caused by interband transitions of core electrons. Because the crystals studied here encompass three different crystal structures, it is possible to correlate the shape of the core interband spectra with not only the crystal structure, but in fact with the nearest-neighbor coordination of the $+$ ions. The broadening of valence- and conduction-band energies by lattice vibrations at elevated temperatures produces strong temperature dependence of interband as well as excitonic structures throughout the spectral region. The inherent sharpness of the optical structures in ionic crystals, which allows the temperature broadening to be observed, is attributed to the strong ionic character and localization of the crystal eigenstates, because these properties produce fairly sharp interband densities of states as well as excitons.

I. INTRODUCTION

The fundamental optical properties of ionic crystals have been extensively studied since the initial absorption measurements were carried out on alkali halides by Hilsch and Pohl¹ in 1930. The large band gaps (5–12 eV) of these crystals place their fundamental absorption region in the vacuum-ultraviolet portion of the spectrum, where experimental work is difficult.² Most measurements have been limited to the region above 1050 Å (below about 12 eV), where LiF windows and reasonably intense hydrogen discharge sources can be used. As a result, these measurements probe only the lowest-energy portion (a few eV) of the fundamental absorption region. At higher photon energies, the experimental problems are much more serious. The continuum spectra from the rare gas discharge sources commonly used are weak, and the stronger emission lines in the spectra do not allow high resolution. Finally, since no known solids are transparent below 1050 Å, a window cannot be used to separate the experimental chamber vacuum from the gas discharge source. The resulting pressure at the sample is too high ($\approx 10^{-6}$ Torr) to carry out low-temperature reflectance measurements, because the residual gases condensed on the cold sample surface cause serious absorption and scattering of far-ultraviolet light.

The use of synchrotron-radiation sources³ re-

moves most of the limitations which conventional gas discharge sources impose on vacuum-ultraviolet spectroscopy. Synchrotron radiation from an accelerated beam of relativistic charged particles provides an intense polarized continuum spectrum of light covering the entire vacuum-ultraviolet range. Furthermore, since the source itself is maintained in ultrahigh vacuum, similar conditions can be reached at the sample (pressure $\approx 10^{-9}$ Torr) and low-temperature measurements can be made throughout the entire spectral region.

We use as a light source in the vacuum ultraviolet the synchrotron radiation from the 240-MeV electron storage ring⁴ at the University of Wisconsin Physical Science Laboratory. This source is at least two orders of magnitude more intense than conventional gas discharge sources in the far ultraviolet (below 1000 Å).⁵ Hence it provides an ideal opportunity to investigate the temperature-dependent optical properties of ionic crystals over a broad energy range.

The optical properties of ionic crystals are not only rich in structure, but the origin of these features presents a challenging theoretical problem. Although a rather large number of band-structure calculations have been carried out,^{6–15} these alone cannot explain the observed spectra. This is because the Coulomb interaction between an electron and a hole excited by the absorption of a photon is only weakly screened, so that strong exciton ef-

fects, as well as interband transitions, are present in the spectra. The exciton problem itself has been given extensive theoretical treatment.¹⁶ Although the relation between excitons and interband transitions in the absorption spectrum has been studied,¹⁷⁻²¹ there has been no theoretical calculation of a complete optical spectrum which includes both effects simultaneously. At higher photon energies at which electrons in core levels are excited, the relative importance of excitons and interband transitions is even more difficult to assess, because the core excitons have sufficient energy to decay by nonradiative processes as well as by direct radiative recombination. The purpose of the present work is (a) to use synchrotron radiation to measure and compare the temperature-dependent optical spectra of a number of ionic crystals over a broad energy region and (b) to analyze what these results suggest about excitons and band-structure effects in these crystals.

This paper reports measurements of the normal-incidence reflectance spectra of KCl, KBr, RbCl, CsCl, CsBr, CaF₂, SrF₂, and BaF₂ in the photon energy range $6 \text{ eV} < \hbar\omega < 36 \text{ eV}$ for temperatures $90^\circ \text{K} < T < 400^\circ \text{K}$. (A preliminary account of this work has been given elsewhere.²²) These results extend the range of both energy and temperature for which the optical spectra of these crystals are known. Although all of these crystals have been studied below 12 eV,²³⁻²⁹ at low as well as at room temperature, experimental work above 12 eV has been more limited. Thin-film absorption measurements have been carried out on the Rb and K halides³⁰⁻³³ and on CsCl and CsBr,³⁰ while reflectance measurements have been limited to RbCl,³⁴ the K halides,³⁵⁻⁴⁰ and CaF₂.^{41,42} Furthermore, only recently have low-temperature data been obtained above 12 eV, on the Rb halides (absorption)³³ and on the K halides (absorption³³ and reflectance⁴³). Moreover, in many cases the measurements presented here reveal much more detail than had previously been reported. With this high sensitivity we investigate and compare the far-ultraviolet reflectance spectra of a group of ionic crystals which encompasses three different cubic crystal structures. The dependence of the observed spectra on temperature, crystal structure, and chemical composition is used extensively in the analysis of the electronic properties of the ionic crystals.

A brief discussion of band structure and exciton properties is given in Sec. II. The experimental techniques are explained in Sec. III, and the results are presented in Sec. IV. These results are discussed in detail and interpreted in Secs. V-VIII. Finally, in Secs. IX-XI we analyze the implications of these results for the fundamental questions posed by the optical spectra and electronic structure of ionic crystals.

TABLE I. SO splittings of atomic levels (eV).

K(3 <i>p</i>)	0.27 ^a	Ca(3 <i>p</i>)	0.0 ^b
Rb(4 <i>p</i>)	0.8 ^b	Sr(4 <i>p</i>)	0.0 ^b
Cs(5 <i>p</i>)	1.7 ^b	Ba(5 <i>p</i>)	2.0 ^b
F(2 <i>p</i>)	0.03 ^c	Br(4 <i>p</i>)	0.31 ^c
Cl(3 <i>p</i>)	0.07 ^c		

^aD. Blechschmidt, R. Klucker, and M. Skibowski, Phys. Status Solidi **36**, 625 (1969).

^bJ. A. Bearden and A. F. Burr, Rev. Mod. Phys. **39**, 128 (1967).

^cJ. C. Phillips, Phys. Rev. **136**, A1705 (1964).

II. THEORETICAL CONSIDERATIONS

Although the crystals investigated here encompass three different crystal structures, the most important features of the electronic structure are common to all of the ionic crystals. In forming the solid, electrons are transferred from the *s* states of the metal atom (alkali or alkaline earth) to the *p* states of the halide atom. This produces positive (metal) and negative (halide) ions, both of which have fully occupied *p* states as their outermost electron shell. Viewed in a simple way the reverse electron-transfer process corresponds to the electronic excitation of the lowest possible energy, in which electrons from the top of the valence bands are excited into the bottom of the conduction bands. Band-structure calculations⁸⁻¹⁵ for the ionic crystals show that the valence bands, originating from the filled *p* states of the - ions, are about 0.75 eV wide. The corresponding wave functions are considerably localized on the - ion sites and have a strong *p* character.^{8,14} Below the valence bands, the *p* core bands from the + ions are flat (completely localized in real space on the + ion sites).⁴⁴ Table I lists the spin-orbit (SO) splittings of the atomic *p* states from which the valence and core bands originate. The excited *s* states of the + ions form the basis for a set of conduction bands. A feature common to the ionic crystals studied here is the existence of excited *d* states of the + ions, lying close in energy to the *s* states. These *d* states produce a second set of conduction bands in the crystal, beginning within 2 eV above the minimum of the *s* bands. These two sets of bands dominate the lowest 6 eV or so of the conduction-band density of states.⁴⁵ Because the wave functions for these conduction bands largely retain their atomic *s* and *d* character,^{7,8,14} one can speak separately of *s*-like and *d*-like conduction bands. Overlap of the ionic wave functions from different sites causes the broadening of ionic energy levels into bands and some transfer of conduction-band charge density from the + ion to the - ion sites.⁴⁶ This charge density remains rather localized near the lattice sites.⁷ Because the electronic states in the crys-

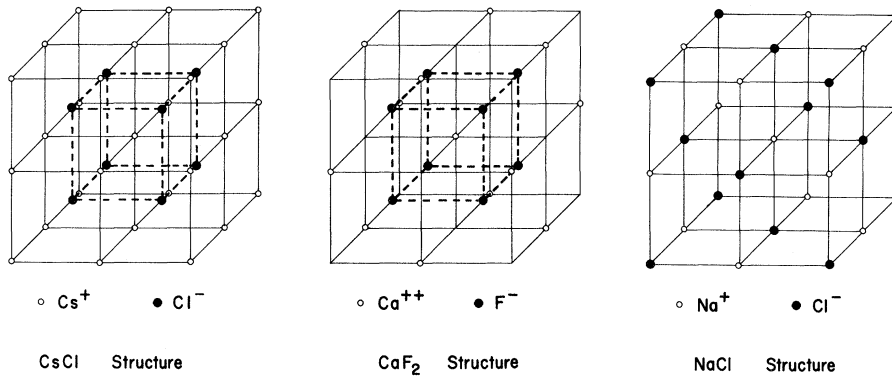


FIG. 1. Structures of the crystals studied in the present work.

tal can be identified with excited states of the ions, interpretation of the optical spectra is greatly aided by comparing the results for chemically related compounds.

The basic electronic properties described above are manifested in somewhat different ways in the energy bands which correspond to the different crystal structures, depicted in Fig. 1. KCl, KBr, and RbCl have a fcc structure (the NaCl or rock-salt structure). A schematic diagram incorporating the main features of the band structure⁶⁻¹³ of these crystals relevant to the present experiment is shown in Fig. 2. Double group notation is used only where SO splittings are large enough to be observed; elsewhere, the single group notation is employed. The primary ionic parentage of the bands at Γ ($\vec{k}=0$) is indicated at left. SO splitting of the valence band produces two levels at Γ , Γ_8^- and Γ_6^- , which correspond respectively to the $j=3/2$ and $j=1/2$ compo-

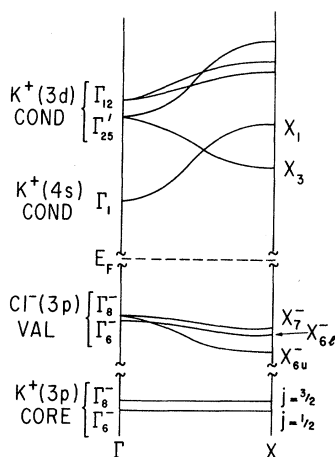


FIG. 2. Schematic band structure (along the [100] axis) of a typical fcc alkali halide. The atomic origin of the conduction, valence, and core bands at Γ is indicated at left, using KCl as an example. E_F is the Fermi energy. Double group notation is used only where SO splittings are large enough to be observed; elsewhere, the single group notation is employed.

ments of the p ion states. Away from Γ , the degeneracy of the $j=3/2$ band is lifted by the crystal potential. The SO-split core levels remain flat because these states are essentially unaffected by the crystal potential. The s -like conduction bands have a minimum at Γ_1 , while the minimum of the d bands is at X_3 , somewhat higher in energy than Γ_1 . The crystal field splits the d bands at Γ into two levels, Γ_{25}' and Γ_{12} , the former at lower energy.

CaF_2 , SrF_2 , and BaF_2 have the fcc fluorite (or CaF_2) structure shown in Fig. 1. Accordingly the Brillouin zone is the same as that for the rocksalt crystals. Energy band calculations have not been carried out for these crystals, and the ordering of levels is uncertain.^{29, 42, 47} In the present discussion the conduction bands are assumed to be similar to those in KCl. The resulting schematic band structure is indicated in Fig. 3. The SO splitting of the F^- valence bands is too small to be observed (0.03 eV in the atom, Table I) so that Γ_8^- and Γ_6^- are

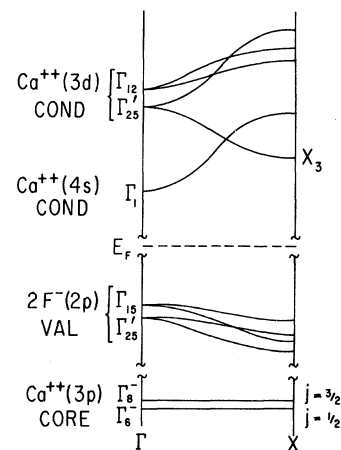


FIG. 3. Schematic band structure (along the [100] axis) of a typical alkaline-earth fluoride. The atomic origin of the bands at Γ is indicated at left, using CaF_2 as an example.

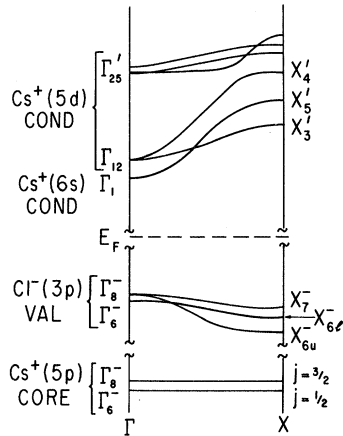


FIG. 4. Schematic band structure (along the [100] axis) of a typical simple cubic Cs halide. The atomic origin of the bands at Γ is indicated at left, using CsCl as an example.

combined into a single level Γ_{15} . However, the presence of two F^- ions per alkaline-earth ion produces an additional set of valence bands associated with Γ'_{25} .^{29,47} Electrical dipole transitions from this state to Γ_1 , Γ'_{25} , and Γ_{12} are parity forbidden.⁴⁷

CsCl and CsBr have the simple cubic CsCl structure (see Fig. 1) and therefore a different Brillouin-zone geometry from the other crystals (the difference is not apparent along the [100] axis depicted in Figs. 2-4). Although the valence and core bands along ΓX (see Fig. 4) are similar to those in KCl, band-structure calculations^{14,15} indicate that the d -like conduction bands have their minimum at Γ_{12} (below Γ'_{25}).⁴⁸ In comparison with KCl, the separation between Γ_{12} and Γ'_{25} is increased and the d -band minimum is closer in energy to the absolute minimum of the conduction bands at Γ_1 .

The optical spectra exhibit features which are determined mainly by the joint density of (initial and final) states and to a lesser extent by matrix element effects. Since the core levels are flat, structures which arise from the excitation of core electrons reflect mostly the density of final states. Where the spectra are not overly complicated by the presence of many different features close in energy, SO splitting of the initial p states may produce an observable duplication of structures. In the one-electron picture, the optical-absorption spectra result from electronic transitions from filled to unfilled band states. However, additional features can arise from absorption in which excitons (bound states of the electron-hole pair) are created. These processes make a significant contribution to the optical spectra of ionic crystals.

When an electron is excited from a filled band, it is subject not only to the crystal potential of the one-electron Hamiltonian, but also to the screened

Coulomb field of the hole which remains

$$V(r_e) = -e^2/\epsilon |r_e - r_h|, \quad (1)$$

where ϵ is the dielectric constant screening the interaction and r_e and r_h are the electron and hole positions. This final-state interaction can produce bound states of the electron-hole pair (or excitons) associated with prominent interband transitions. The exciton wave function is composed of electron and hole states in the conduction and valence bands. In the Wannier model,⁴⁹ the Coulomb interaction (1) is treated as a perturbation on the one-electron band scheme, so that in the effective-mass approximation,⁵⁰ excitons are formed with energies given by

$$E_n(\vec{K}) = -\frac{\mu e^4}{2\hbar^2 \epsilon^2} \frac{1}{n^2} + \frac{\hbar^2 \vec{K}^2}{2(m_e + m_h)}, \quad (2)$$

relative to an energy zero at the conduction-band critical point with which the exciton is associated. In (2), the quantum number n is the exciton band index, \vec{K} is the exciton wave vector, and m_e and m_h are the effective masses of the electron and hole. The exciton reduced mass is $\mu = m_e m_h / (m_e + m_h)$. The first term produces a hydrogenic series of levels with a binding energy of the lowest state (in eV)

$$E_B \equiv E_1(0) = \frac{13.6 (\mu/m_0)}{\epsilon^2}, \quad (3)$$

where m_0 is the free-electron mass. The exciton radius (approximately the mean electron-hole separation) in \AA is then

$$a = \frac{\hbar^2 \epsilon}{\mu e^2} = 0.5 \frac{\epsilon}{(\mu/m_0)}. \quad (4)$$

The oscillator strength f of the exciton absorption band increases with larger exciton binding energy or shorter radius (for hydrogenic s states of the exciton, $f \propto a^{-3}$),⁵¹ and the strength of the interband transition with which the exciton is associated is reduced accordingly to conserve oscillator strength. Dispersion of the exciton bands is given by the second term in (2). Since the photon wave vector is small compared to Brillouin-zone dimensions, light can only excite $\vec{K} = 0$ states of the exciton. States with $\vec{K} \neq 0$ can be reached, e. g., by phonon-assisted optical transitions.

The Wannier model is valid in semiconductors where dielectric constants are large (≈ 16) and the resulting exciton binding energies are small compared to the band gap. In ionic crystals, however, the static dielectric constant $\epsilon_0 \approx 5$ gives $E_B \approx 0.25$ eV and $a \approx 5 \text{\AA}$ for $\mu = 0.5m_0$. This implies an orbital frequency of the electron about the hole (of order $\omega = 10^{15}$ rad/sec) much larger than the characteristic phonon frequencies (of order 3×10^{13} rad/sec),¹⁶ so that the ions cannot respond to screen

the interaction. Accordingly, the optical dielectric constant $\epsilon_\infty \approx 2.5$ is more appropriate, so $E_B \approx 1.1$ eV and $a \approx 2.5 \text{ \AA} \approx$ the interionic spacing.⁵² As a result, the Wannier model is not strictly valid; the screening is nonuniform and exciton effects are very strong. In fact, the Frenkel model⁵³ for tightly bound excitons or an intermediate case¹⁶ may be more correct. Although these alternative descriptions of excitons in ionic crystals have also been applied, the Wannier model is most often used because it can be straightforwardly related to one-electron band structures.

III. EXPERIMENTAL TECHNIQUES

Synchrotron radiation from the 240-MeV electron storage ring at the University of Wisconsin⁴ is used as a light source for vacuum-ultraviolet spectroscopy in the photon energy range 6–36 eV. The experimental system is described in detail elsewhere. The rotating light pipe scanning reflectometer technique⁵⁴ is used to obtain continuous reflectance spectra at near-normal ($\approx 6^\circ$) incidence as the wavelength region is scanned. The front surface of the quartz light pipe is coated with sodium salicylate, which fluoresces in the blue (peak at 4200 \AA) when excited by vacuum-ultraviolet photons.² Some of the fluorescent light is transmitted down the light pipe by total internal reflection and out of the vacuum through a window to the photomultiplier. The light pipe is shaped so that it captures alternately the full incident and reflected beams as it is rotated about its central axis at about 30 Hz by a magnetically coupled feedthrough. The time-dependent current from the photomultiplier is processed by an electronic gating circuit which separates the signals produced by the incident and the reflected light beams and subtracts the dark current from each channel. A feedback system controls the high voltage applied to the photomultiplier in such a way that the photocurrent corresponding to the incident beam is kept constant. In this way the reflectance can be measured directly as the wavelength region is scanned. In the vacuum-ultraviolet region, weak structures in the reflectance (of order $\Delta R = 0.1\%$ or less) are easily observed. The reflectance spectra are recorded simultaneously in analog form on a strip-chart recorder as well as in digital form on magnetic tape, to allow direct computer processing for corrections, analysis, and plotting.

Alignment of the sample surface is accomplished using first-order light from the grating. The light pipe is turned toward the sample so that the photomultiplier measures the intensity of light reflected from the sample onto the front surface of the light pipe. Then the orientation of the sample is adjusted to maximize this reflected intensity. The samples are baked at about 130 $^\circ\text{C}$ in the ultrahigh vacuum for at least 12 h before measurement in order to

remove adsorbed gases from their surfaces. With these procedures, reflectance magnitudes are reproducible to about $\Delta R = \pm 1\%$. Furthermore, the reflectance magnitudes, averaged over the structures in the spectrum, do not depend on time or on sample temperature. Thus the far-ultraviolet reflectance spectra show no sign of contamination of the sample surface by residual gases, even at low temperature.

Single crystals⁵⁵ of KCl, KBr, CaF_2 , SrF_2 , and BaF_2 were cleaved just prior to mounting in the experimental chamber. A sample of RbCl was obtained⁵⁶ with a cleaved surface. A CsCl crystal was grown in our laboratory by pulling from the melt; this sample was polycrystalline because CsCl undergoes a phase transition from NaCl to CsCl structure upon cooling from high temperature. Since they do not cleave, CsCl and CsBr⁵⁷ were mechanically polished. To prevent adsorption of water, mineral oil was used as an inert vehicle for the polishing paste. The samples were then stored in the oil until use. Just before mounting, they were rinsed in fresh methanol. Since they absorb water, all alkali halides were kept above room temperature by a heat lamp from the time their surfaces were prepared until they were mounted in the experimental chamber.

IV. EXPERIMENTAL RESULTS

The near-normal incidence reflectance spectra of KCl, RbCl, CsCl, CsBr, CaF_2 , SrF_2 , and BaF_2 are shown in Fig. 5. The measurements cover the photon energy range $6 \text{ eV} < \hbar\omega < 36 \text{ eV}$ for temperatures $90^\circ\text{K} < T < 400^\circ\text{K}$. Correction has been made for second-order light from the grating. The wavelength resolution is $\Delta\lambda = 5 \text{ \AA}$. To separate the spectra corresponding to different sample temperatures, the low- and high-temperature curves have been shifted vertically by an amount $+RS$ and $-RS$, respectively, so that curves for 90°K appear above and those for 400°K appear below the 300°K measurements. The magnitude of RS for each crystal is indicated by a vertical bar in the figure as well as being given in the figure caption. This procedure is followed for all the reflectance spectra presented in this work.

The absolute magnitudes of the reflectance peaks reported by different workers for ionic crystals in the vacuum ultraviolet differ by several percent. These small discrepancies are to be expected because of differences in the conditions of the sample surfaces and of errors associated with the optical techniques used. In contrast, we reported reflectance values recently²² which were generally higher than those of other workers by an amount several times larger than these expected variations. We have since determined that those values were erroneously enhanced by alignment errors of the light

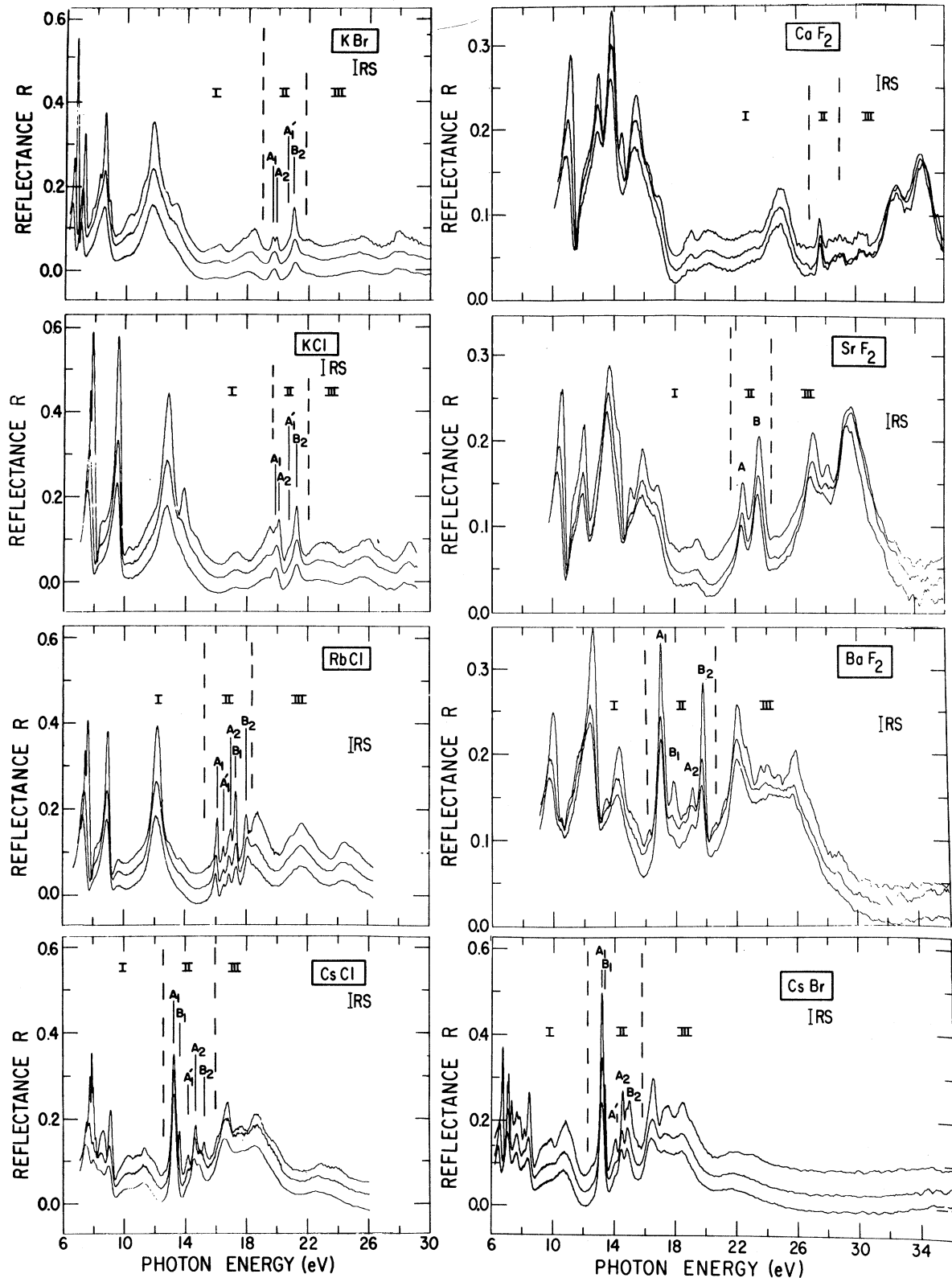


FIG. 5. Near-normal incidence ($\approx 6^\circ$) reflectance spectra of several ionic crystals in the far ultraviolet. Vertical shifts of $\pm RS$ respectively separate the 90°K spectra (above) and the 400°K spectra (below) from the spectra taken at 300°K . The wavelength resolution is $\Delta\lambda = 5 \text{ \AA}$. $RS = 0.035$ for the alkali halides and $RS = 0.0175$ for the alkaline-earth fluorides.

pipe. Furthermore, deterioration of the sensitivity of portions of the sodium salicylate coating on the light pipe (perhaps due to aging in the ultrahigh-vacuum environment, heat from the samples being baked, or radiation damage) was not readily detected and corrected for in the incident beam alignment, because frequent checks of the light pipe alignment were not possible at that time. (In contrast, alignment of the sample to optimize the position of the reflected beam on the light pipe was carried out for each sample at each temperature.) This deficiency has been corrected. We found that the original measurements²² are correct within an error of $\pm 2\%$ after all reflectance values are multiplied by 0.7. This correction has been applied to the data discussed in the present paper.

For analyzing the electronic structure, the position and shape of features in the reflectance spectra are more important than are the actual reflectance magnitudes. The characteristics of the spectra above the fundamental absorption edge suggest a natural division into three regions, which are separated by dashed vertical lines in Fig. 5.

Structure in region I arises from optical excitation of electrons in the valence bands, which are formed primarily from the filled p states of the $-$ ions (the halides). It is generally accepted that the structures at lower energy in the valence excitation region are caused by exciton absorption, while interband transitions dominate at higher energies in region I. Valence excitations may continue into regions II and III, but they should be weaker there since the oscillator strength of valence electrons must decrease at higher energy. In principle this can be checked by evaluating the effective number of electrons from optical constants determined by Kramers-Kronig analysis of the reflectance data.

At higher photon energies, electrons are excited from core states which lie below the valence bands. The core levels investigated in this experiment are the p states of the $+$ ions (alkali and alkaline earth). Region II, several eV wide, begins with the onset of these core excitations. The spectra in this region are characterized by a number of very sharp peaks. The finite wavelength resolution of the monochromator prevents a determination of the true widths of these peaks, which must be ≤ 0.2 eV. An abrupt change to broader structures (widths > 0.5 eV) occurs on passing from region II to III, where the features are also caused primarily by excitations of the core states of the $+$ ions.

One may expect that the reflectance spectrum in the core excitation region, like that in the valence region, involves both excitons (at lower energies) and interband transitions (which should dominate at higher energies). The p core electrons excited in these measurements lie in the outer shell of the

$+$ ions. As a result, the core exciton lifetime may be comparable to that of the valence exciton, so that strong core excitons appear in the spectra. The large mass of the core hole should produce narrow core exciton absorption bands. Indeed, the sharpness of the reflectance peaks in region II suggests that these features are due to core excitons,^{31,37,38,58,59} in contrast to the considerably broader structures which are observed in region III. In the discussion which follows, we assume that absorption by core excitons dominates the spectra in region II, while structure in region III arises primarily from interband transitions of core electrons. This assignment is examined in detail in Sec. IX.

Tables II-IV list the energies (at 90°K) of prominent features in the spectra, as well as their characteristics and identification where possible. Shifts in energy with temperature can be determined only for sharp peaks, whose position can be accurately located. The energies of such peaks at various temperatures are given in Table V.

V. ONSET OF CORE EXCITATIONS

To analyze the results, it is necessary to assign structures in the reflectance spectra to either valence or core electron excitation. At photon energies sufficiently large to cause absorption by core electrons, valence excitations should have small oscillator strengths because of the high kinetic energy of the upper conduction-band states (rapid oscillation of the wave functions). Therefore, the core onset—defined here as the lowest energy at which there appears a strong core excitation structure—is a useful guideline for separating core from valence excitation structures.

Since the low-lying conduction bands are associated primarily with states of the $+$ ions, the energy of core excitation structures near the core onset should be insensitive to the identity of the halide, while the position of valence excitation features will depend strongly on the halide. This characteristic can be used to identify the core onset. As seen in Fig. 5, the position of the A_1 peak in KBr and KCl (at 19.7 and 19.9 eV, respectively) depends very little on the halide. Thus the $K^+(3p)$ core onset^{30,37,38} is located at about 19.8 eV. The position of the A_1 peak in CsCl and CsBr is also insensitive to the halide,³⁰ so that the $Cs^+(5p)$ onset is at 13.25 eV. The A_1 peak in RbCl occurs at very nearly the same energy as a similar structure observed by other workers³⁰ in RbBr and RbI, so that the $Rb^+(4p)$ onset is at 16.1 eV.

Similar data for comparing the optical spectra of alkaline-earth compounds having different halides are not yet available. However, it appears that the core onset is generally characterized by the appearance of very sharp structure. Accord-

TABLE II. Energies (at 90 °K), characteristics, and identifications of prominent features in the reflectance spectra of KCl, KBr, and RbCl.

KCl		KBr		RbCl	
$\hbar\omega$ (eV)		$\hbar\omega$ (eV)		$\hbar\omega$ (eV)	
7.72	$\Gamma_8^- \rightarrow \Gamma_1$ exciton	6.75	$\Gamma_8^- \rightarrow \Gamma_1$ exciton	7.47	$\Gamma_8^- \rightarrow \Gamma_1$ exciton
7.88	$\Gamma_6^- \rightarrow \Gamma_1$ exciton	7.26	$\Gamma_6^- \rightarrow \Gamma_1$ exciton	7.64	$\Gamma_6^- \rightarrow \Gamma_1$ exciton
8.40	higher Γ exciton	7.79	shoulder, $\Gamma_8^- \rightarrow \Gamma_1$ band edge	8.10	higher Γ exciton
8.55	higher Γ exciton	8.26	$X_7^- \rightarrow X_3$ exciton	8.29	higher Γ exciton
9.57	$X_5^- \rightarrow X_3$ exciton	8.62	$X_{6f}^- \rightarrow X_3$ exciton	8.93	$X_5^- \rightarrow X_3$ exciton
10.31	weak peak	8.93	$X_{6u}^- \rightarrow X_3$ exciton	9.61	weak peak
11.45	weak shoulder	9.45	weak shoulder	10.9	weak shoulder
12.87	strong peak	10.35	weak peak	12.17	strong peak
13.89	peak—very strong temp. dep.	11.15	shoulder	12.95	weak shoulder
14.70	weak shoulder	11.81	strong peak	13.63	weak peak
17.34	peak	12.4	weak shoulder	15.7	weak shoulder
19.53	peak	12.69	weak shoulder	16.11	$\text{Rb}^+(4p, j = \frac{3}{2}) \rightarrow \Gamma_1$ core exciton
19.92	$\text{K}^+(3p, j = \frac{3}{2}) \rightarrow \Gamma_1$ core exciton	13.30	peak	16.50	higher core exciton
20.13	$\text{K}^+(3p, j = \frac{1}{2}) \rightarrow \Gamma_1$ core exciton	15.5	weak shoulder	16.85	weak shoulder
20.7	shoulder	16.20	peak	17.00	$\text{Rb}^+(4p, j = \frac{1}{2}) \rightarrow \Gamma_1$ core exciton
21.28	$\text{K}^+(3p) \rightarrow X_3$ core exciton	17.3	weak shoulder	17.29	$\text{Rb}^+(4p, j = \frac{3}{2}) \rightarrow X_3$ core exciton
23.0	peak	17.7	weak shoulder	17.99	$\text{Rb}^+(4p, j = \frac{1}{2}) \rightarrow X_3$ core exciton
25.9	peak	18.47	peak	18.7	strong peak
28.7	peak	19.72	$\text{K}^+(3p, j = \frac{3}{2}) \rightarrow \Gamma_1$ core exciton	20.8	shoulder
		19.97	$\text{K}^+(3p, j = \frac{1}{2}) \rightarrow \Gamma_1$ core exciton	21.63	peak
		20.7	weak shoulder	22.3	weak shoulder
		21.15	$\text{K}^+(3p) \rightarrow X_3$ core exciton	24.45	peak
		22.1	shoulder		
		25.6	peak		
		28.0	peak		

ingly, one can tentatively place the core onsets in the alkaline-earth fluorides at the following energies (see Fig. 5): $\text{Ca}^{++}(3p) = 27.7$ eV, $\text{Sr}^{++}(4p) = 22.5$ eV, and $\text{Ba}^{++}(5p) = 17.1$ eV.

The core onset energies can be compared with the electron spectroscopy for chemical analysis (ESCA) data of Siegbahn *et al.*⁶⁰ In these experiments, x rays incident on the solid cause the emission of electrons with large kinetic energies. By

measuring these kinetic energies, the binding energies of electrons in different bands in the crystals can be determined. The electron kinetic-energy scale is normalized by comparing the binding energy of valence electrons to the valence \rightarrow conduction-band edge as determined by recombination luminescence at low temperature.⁶¹ The ESCA data locate the $\text{K}^+(3p)$ core level at 20.5 and 20.6 eV below the bottom of the conduction bands in KCl and KBr,

TABLE III. Energies (at 90 °K), characteristics, and identifications of prominent features in the reflectance spectra of CsCl and CsBr.

CsCl		CsBr	
$\hbar\omega$ (eV)		$\hbar\omega$ (eV)	
7.78	$\Gamma_8^- \rightarrow \Gamma_1$ exciton	6.77	$\Gamma_8^- \rightarrow \Gamma_1$ exciton
7.90	$\Gamma_8^- \rightarrow \Gamma_{12}$ exciton	7.12	$\Gamma_8^- \rightarrow \Gamma_{12}$ exciton
7.97	$\Gamma_6^- \rightarrow \Gamma_1$ exciton	7.18	$\Gamma_6^- \rightarrow \Gamma_1$ exciton
8.05	shoulder	7.35	peak
8.16	$\Gamma_6^- \rightarrow \Gamma_{12}$ exciton	7.68	$\Gamma_6^- \rightarrow \Gamma_{12}$ exciton
8.64	peak	7.87	shoulder
9.12	peak	8.18	peak
9.60	shoulder	8.51	peak
10.25	peak	9.3	shoulder
11.30	peak	9.91	peak
12.0	shoulder	10.6	shoulder
12.6	weak shoulder	10.87	peak
13.27	$\text{Cs}^*(5p, j=\frac{3}{2}) \rightarrow \Gamma_1$ core exciton	11.3	shoulder
13.63	$\text{Cs}^*(5p, j=\frac{3}{2}) \rightarrow \Gamma_{12}$ core exciton	12.5	weak shoulder
14.21	higher core exciton	13.23	$\text{Cs}^*(5p, j=\frac{3}{2}) \rightarrow \Gamma_1$ core exciton
14.66	$\text{Cs}^*(5p, j=\frac{1}{2}) \rightarrow \Gamma_1$ core exciton	13.42	$\text{Cs}^*(5p, j=\frac{3}{2}) \rightarrow \Gamma_{12}$ core exciton
15.24	$\text{Cs}^*(5p, j=\frac{1}{2}) \rightarrow \Gamma_{12}$ core exciton	14.15	higher core exciton
16.0	weak shoulder	14.59	$\text{Cs}^*(5p, j=\frac{1}{2}) \rightarrow \Gamma_1$ core exciton
16.12	shoulder	14.8	shoulder
16.79	peak	15.03	$\text{Cs}^*(5p, j=\frac{1}{2}) \rightarrow \Gamma_{12}$ core exciton
17.65	peak	15.5	shoulder
18.65	peak	16.55	peak
20.0	shoulder	17.2	shoulder
22.9	peak	17.51	peak
23.9	shoulder	18.47	peak
		19.0	shoulder
		22.0	peak

respectively.⁶⁰ This places the core interband edge between the (A_1, A_2) doublet and the B_2 peak, near the A_1' shoulder (see Fig. 5). Thus the ESCA data suggest that peaks A_1 and A_2 in KCl and KBr are caused by core exciton absorption, because they lie below the core interband edge. Further ESCA measurements on other ionic crystals will be useful.

The separation in energy between the p core levels and the Fermi energy in the alkali and alkaline-earth metals can be obtained from x-ray data.⁶² Table VI lists these atomic x-ray levels E_x as well as the core onset energies E_0 in the metal halides, as determined from the reflectance data in Fig. 5. The difference $E_x - E_0$ is also tabulated (using the lower-energy component of SO-split pairs of x-ray levels). Because the alkali (or alkaline-earth) halides are isoelectronic, one expects a reasonably simple relation between E_0 and E_x . The difference $E_0 - E_x$ is about 2 eV for the alkali halides and about 2.4 eV for the alkaline-earth halides. This approximate consistency throughout the crystals indicates

that the core onset energies determined from the optical data are reasonable.

VI. VALENCE-BAND EXCITATIONS

Structures in region I of the spectra (see Fig. 5) arise from optical excitation of electrons in the valence bands. It is generally accepted that excitons cause the peaks near the fundamental absorption edge, while the shape of structures at higher energies is determined mostly by interband transitions. There are strong similarities between the valence excitation spectra of crystals having the same crystal structure, so the discussion is grouped accordingly.

A. Face-Centered Cubic Alkali Halides

The reflectance spectra of KBr, KCl, and RbCl in the valence excitation region are shown in detail in Figs. 6–8. Three major groups of structure appear in all three crystals, at roughly 7, 9, and 12 eV. The first group is a doublet composed of the $\Gamma_8^- \rightarrow \Gamma_1$ and $\Gamma_6^- \rightarrow \Gamma_1$ excitons (see Fig. 2),^{24,26,63} separated by the SO splitting of the valence bands at Γ . The 0.17-eV splitting in KCl and RbCl is small enough that it is resolved only at low temperature. Exchange interaction⁶³ between electron and hole alters the observed splitting in the chlorides from the free atom value (0.07 eV, Table I) and changes the intensity ratio of the doublet from the 2:1 ratio expected by the statistical weights of the $j=\frac{3}{2}$ and $j=\frac{1}{2}$ components.

The second group of structures (near 9 eV) is not observed in the Na halides.^{24,26,36} Since $2d$ states [above the $\text{Na}^*(3s)$ states] are not possible, the structures near 9 eV have been attributed to excitons associated with the minimum at X_3 of the d -like conduction bands.^{24,26,63} In KBr three excitons, associated with X_7^- , X_{6u}^- , and X_{6l}^- , are observed (see Fig. 2). However, the SO splitting of the $\text{Cl}^*(3p)$ valence band is sufficiently small compared to the crystal-field splitting at X that only two levels, X_5' and X_4' , are present in KCl and RbCl. Since electric dipole transitions $X_4' - X_3$ are forbidden, only one X exciton is observed in KCl and RbCl.⁶³ The separation between the Γ and X excitons is smaller in RbCl than in KCl, in agreement with the trend²⁶ that d -like conduction bands move to lower energy (closer to the s bands) with heavier alkali ions.

The third group of prominent valence structures is dominated by a strong peak which occurs at 12.87, 11.81, and 12.17 eV in KCl, KBr, and RbCl, respectively. In KCl and RbCl a very weak shoulder appears on the low-energy side, while two stronger shoulders arise in KBr. Two shoulders appear at low temperature on the high-energy side of the main peak. In KCl the shoulder just above the main peak sharpens drastically at low temperature. These higher-energy valence excitation structures are not

TABLE IV. Energies (at 90 °K), characteristics, and identifications of prominent features in the reflectance spectra of CaF₂, SrF₂, BaF₂.

CaF ₂	SrF ₂	BaF ₂
$\hbar\omega$ (eV)	$\hbar\omega$ (eV)	$\hbar\omega$ (eV)
11.18 $\Gamma_{15} \rightarrow \Gamma_1$ exciton	10.60 $\Gamma_{15} \rightarrow \Gamma_1$ exciton	10.00 $\Gamma_{15} \rightarrow \Gamma_1$ exciton
12.1 $\Gamma_{15} \rightarrow \Gamma_1$ band edge	11.25 $\Gamma_{15} \rightarrow \Gamma_1$ band edge	10.57 higher exciton
13.04 X_3 exciton	12.02 X_3 exciton	11.0 $\Gamma_{15} \rightarrow \Gamma_1$ band edge
13.93 peak	13.71 peak	11.7 X_3 exciton
14.57 peak, very temp. dep.	14.35 shoulder	12.66 peak
15.53 peak	15.07 peak, very temp. dep.	13.50 peak, very temp. dep.
16.4 shoulder	15.86 peak	14.34 peak
16.98 weak peak	16.80 peak	15.5 shoulder
19.12 peak	19.40 peak	16.35 weak peak
20.35 peak	22.47 $\text{Sr}^{++}(4p) \rightarrow \Gamma_1$ core exciton	17.10 $\text{Ba}^{++}(5p, j = \frac{3}{2}) \rightarrow \Gamma_1$ core exciton
23.3 shoulder	23.56 $\text{Sr}^{++}(4p) \rightarrow X_3$ core exciton	17.3 shoulder
25.10 $\text{F}^-(2s)$ core excitation?	24.7 weak peak	17.95 $\text{Ba}^{++}(5p, j = \frac{3}{2}) \rightarrow X_3$ core exciton
27.70 $\text{Ca}^{++}(3p) \rightarrow \Gamma_1$ core exciton	27.14 strong peak	19.19 $\text{Ba}^{++}(5p, j = \frac{1}{2}) \rightarrow \Gamma_1$ core exciton
29.1 weak peak	28.13 weak peak	19.89 $\text{Ba}^{++}(5p, j = \frac{1}{2}) \rightarrow X_3$ core exciton
30.5 weak peak	29.70 strong peak	20.6 weak peak
32.85 strong peak		21.3 shoulder
34.50 strong peak		22.13 peak
		22.72 shoulder
		23.69 weak peak
		24.1 weak peak
		24.9 weak peak
		26.00 peak
		27.2 shoulder
		28.9 shoulder

as well understood as are the Γ and X excitons. Pseudopotential calculations of the one-electron band structure and optical spectrum of KCl¹² show strong structure starting near 10 eV, which indicates that interband transitions are important in the 12-eV structures. The calculations suggest that the weak shoulder at 11.5 eV in KCl arises primarily from transitions near $\Gamma_{15} \rightarrow \Gamma'_{25}$ and $\Gamma_{15} \rightarrow \Gamma_{12}$, while the strong peak at 12.87 eV involves transitions near Σ (ΓK axis) to energy states above Γ_{12} .¹²

Features in the reflectance caused by valence electron excitation occur at even higher energy in the fcc alkali halides, as seen in Fig. 5. The peaks at 17.34 and 19.53 eV in KCl (which lie below the core onset) shift down about 1 eV to 16.20 and 18.47 eV in KBr. This shift matches the 0.97-eV reduction in the energy of the first exciton. Since the valence bands in these crystals are fairly narrow, these higher-energy valence excitations must involve final states 10 eV or more above the conduction-band minimum. If the two peaks in KCl have the same origin as the peaks in KBr, they cannot be due to $\text{Cl}^-(3s)$ and $\text{Br}^-(4s)$ core excitations, be-

cause these core levels lie at very different energies below the valence bands (10.7 and 22.4 eV, respectively).⁶²

B. Alkaline-Earth Fluorides

The reflectance spectra of CaF₂, SrF₂, and BaF₂ in the valence excitation region are shown in Figs. 9–11. The spectra are composed of a number of fairly strong peaks extending up to about 17 eV (in BaF₂, core excitations begin near 16 eV and are omitted from Fig. 11). Although the structures in Figs. 9–11 are in good agreement with the reflectance measurements of Miyata and Tomiki,²⁹ carried out at 300 °K and at 78 °K up to 12 eV, these authors also observed fine structures about $\Delta R = 1\%$ in magnitude and 5–10 Å in width superimposed on the exciton peaks, using a 1-Å resolution. In this region of the spectrum, the scanning reflectometer⁵⁴ is capable of observing structures ten times smaller than this. Using a 3-Å spectral resolution and repeated slow scans over the wavelength region in question, we were unable to detect any reproducible fine structures such as Miyata and Tomiki reported.

TABLE V. Temperature dependence of the energies (eV) of sharp reflectance peaks. The approximate error is $\Delta E = \pm 0.02$ eV.

400 °K	300 °K	90 °K	400 °K	300 °K	90 °K
	KBr			CaF ₂	
6.44	6.55	6.75	10.85	11.02	11.18
7.01	7.11	7.26	12.92	12.97	13.04
8.53	8.56	8.62	13.79	13.86	13.93
11.71	11.76	11.81	15.37	15.40	15.53
19.79	19.78	{ 19.72	25.00	25.05	25.10
		{ 19.97	27.75	27.75	27.70
21.16	21.13	21.15	32.85	32.85	32.85
			34.50	34.50	34.50
	KCl			SrF ₂	
7.52	7.68	{ 7.72	10.27	10.41	10.60
		{ 7.88	11.91	11.98	12.02
9.48	9.52	9.57	13.55	13.61	13.71
12.72	12.75	12.87	15.80	15.85	15.86
19.86	19.94	{ 19.92	22.37	22.42	22.47
		{ 20.13	23.46	23.50	23.56
21.26	21.28	21.28	26.95	27.10	27.14
			29.40		29.70
	RbCl			BaF ₂	
7.28	7.38	{ 7.47	9.76	9.80	10.00
		{ 7.64	12.46	12.44	12.66
8.89	8.89	8.93	14.24	14.20	14.34
12.05	12.08	12.17	17.09	17.08	17.10
15.98	16.03	16.11	19.14	19.12	19.19
16.55	16.51	16.50	19.80	19.81	19.89
16.87	16.87	17.00	22.10	22.05	22.13
17.34	17.34	17.29			
18.12	18.07	17.99			
	CsCl			CsBr	
7.47	7.58	7.78	6.43	6.56	6.77
	7.74	7.90	7.10	7.08	{ 7.12
7.97	7.97	7.97			{ 7.18
8.98	9.03	9.12	7.65	7.67	7.68
13.29	13.27	13.27	8.35	8.43	8.51
14.63	14.63	14.66	13.23	13.25	13.23
14.89	15.05	15.24	14.52	14.54	14.59
16.64	16.70	16.79	16.43	16.50	16.55
18.60	18.65	18.65	18.42	18.38	18.47

The similarity between the band structure of KCl and that of the alkaline-earth fluorides can be used to make a tentative identification of structures in the latter crystals. The reflectance spectra of MgF₂⁴² show only a single strong peak occurring at nearly the same energy as the lowest peak in CaF₂. Since the MgF₂ conduction bands can have no low-lying *d*-like states [from a Mg⁺⁺(2*d*) level], the higher peaks in CaF₂, SrF₂, and BaF₂ are attributed to transitions associated with *d*-like conduction bands. Thus the lowest peaks (11.18, 10.60, and 10.00 eV in CaF₂, SrF₂, and BaF₂) are assigned to excitons associated with $\Gamma_{15} \rightarrow \Gamma_1$ (see Fig. 3). The shoulder which follows at 12.1 and 11.25 eV in

CaF₂ and SrF₂, respectively, may be the $\Gamma_{15} \rightarrow \Gamma_1$ interband edge. As in KCl, excitons associated with *d*-like states at *X*₃ appear to occur 1.5–2.0 eV above the first exciton (at 13.04 and 12.02 eV in CaF₂ and SrF₂). In BaF₂ the weak peak at 10.57 eV may be an excited state of the first exciton, while the *X*₃ exciton may be subdued, producing only a shoulder at 11.7 eV. The strongest peaks in the valence excitation spectra, at 13.93, 13.71, and 12.66 eV in CaF₂, SrF₂, and BaF₂, may be associated with transitions near $\Gamma_{15} \rightarrow \Gamma'_{25}$, $\Gamma_{15} \rightarrow \Gamma_{12}$, and near Σ (ΓK axis) to states above Γ_{12} . At low temperature, new peaks appear at 14.57 eV in CaF₂, 15.07 eV in SrF₂, and 13.50 eV in BaF₂. Some of

TABLE VI. Comparison of core onset energies and atomic x-ray data. The core onset energies E_0 are determined from the characteristics of the reflectance spectra presented in Fig. 5. The atomic x-ray levels E_x measure the energy separation between the p core states and the Fermi energy in the alkali (or alkaline-earth) metal. The difference $E_0 - E_x$ is given (using the lower-energy component of SO pairs of x-ray levels).

Crystal	E_0 (eV)	E_x (eV) ^a	$E_0 - E_x$ (eV)
KCl	19.9	17.8 ± 0.4	2.1
KBr	19.7	17.8 ± 0.4	1.9
RbCl	16.1	14.0 ± 0.4	2.1
		14.8 ± 0.4	
CsCl	13.25	11.4 ± 0.5	1.85
		13.1 ± 0.5	
CsBr	13.25	11.4 ± 0.5	1.85
		13.1 ± 0.5	
CaF ₂	27.7	25.4 ± 0.4	2.3
SrF ₂	22.5	19.9 ± 0.3	2.6
BaF ₂	17.1	14.6 ± 0.5	2.5
		16.6 ± 0.5	

^aJ. A. Bearden and A. F. Burr, Rev. Mod. Phys. **39**, 128 (1967).

the extra structures in these crystals which do not appear in the spectra of KCl (Fig. 7) may involve transitions from the second set of valence bands associated with Γ'_{25} . Energy band calculations are needed to understand the optical spectra of the alkaline-earth fluorides in detail.

C. Simple Cubic Cs Halides

Although it is possible to produce thin films of CsCl and CsBr in which some portions of the sample have the rocksalt structure,^{23,28,64} the 400 °K annealing used to outgas the surfaces of our bulk samples has been shown²⁴ to produce exclusively the simple cubic CsCl structure depicted in Fig. 1. Accordingly, the schematic band structure shown in Fig. 4 is appropriate to the measurements on CsCl and CsBr presented here. The reflectance spectra of these crystals in the valence excitation region are shown in Figs. 12 and 13. Even though band-structure calculations have been carried out

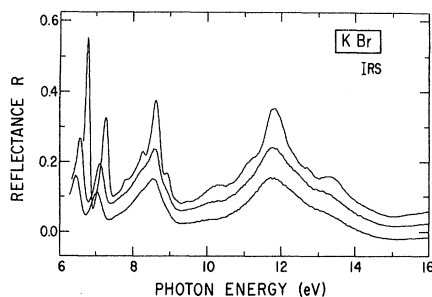


FIG. 6. Reflectance spectra of KBr in the valence excitation region, $RS=0.035$.

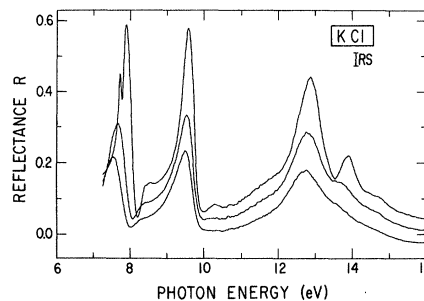


FIG. 7. Reflectance spectra of KCl in the valence excitation region, $RS=0.035$.

for CsI,^{14,15} the complexity of the Cs halide spectra makes their interpretation difficult.

In CsCl, the shoulder at 8.05 eV in the 90 °K reflectance spectrum (Fig. 12) appears as a peak in the 10 °K thin-film absorption data of Teegarden and Baldini.²⁴ They considered this peak and the three peaks below it in energy to be excitons associated with the conduction-band states Γ_1 and Γ_{12} (Fig. 4). The SO splitting of the valence band in CsCl should be approximately equal to that in KCl and RbCl (0.17 eV). Accordingly, the first (7.78 eV) and third (7.97 eV) peaks (separation 0.19 eV) are attributed to $\Gamma'_8 \rightarrow \Gamma_1$ and $\Gamma'_6 \rightarrow \Gamma_1$ excitons. The second peak (7.90 eV) is then the $\Gamma'_8 \rightarrow \Gamma_{12}$ exciton. The very strong temperature dependence of the 8.05-eV shoulder distinguishes it from the other peaks, so that it may be an excited state of the Γ_1 or the Γ_{12} exciton. The peak at 8.16 eV is probably the $\Gamma'_6 \rightarrow \Gamma_{12}$ exciton. With this tentative identification, the separation of the Γ_{12} excitons indicates a larger SO splitting of the valence band than do the Γ_1 excitons.

In CsBr (Fig. 13), Teegarden and Baldini²⁴ suggested that the first and fourth peaks at low temperature (6.77 and 7.35 eV) are $\Gamma'_8 \rightarrow \Gamma_1$ and $\Gamma'_6 \rightarrow \Gamma_1$ excitons, while the second, third, and fifth (7.12, 7.18, and 7.68 eV) are excitons associated with $Cs^*(5d)$ excited states. However, since the minimum of the d -like conduction bands in the simple cubic Cs halides is at Γ_{12} ,^{14,15} only two excitons

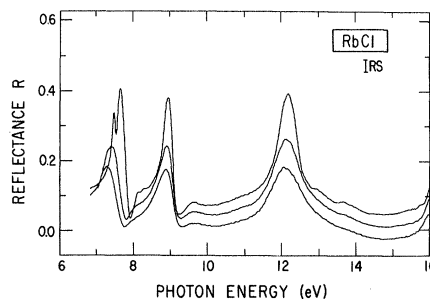


FIG. 8. Reflectance spectra of RbCl in the valence excitation region, $RS=0.035$.

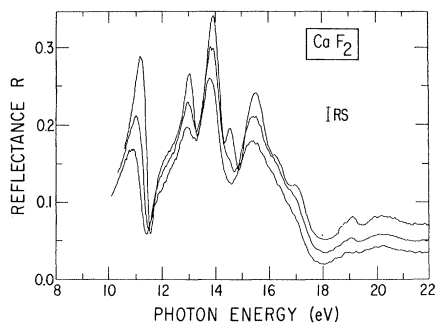


FIG. 9. Reflectance spectra of CaF_2 in the valence excitation region, $RS=0.0175$.

related to the d bands are expected. Gavini and Cardona²⁸ proposed that in CsBr the first three peaks appearing at room temperature (at 6.56, 7.08, and 7.67 eV) are excitons associated with $\Gamma_8^- \rightarrow \Gamma_1$, $\Gamma_6^- \rightarrow \Gamma_1$ degenerate with $\Gamma_8^- \rightarrow \Gamma_{12}$ and $\Gamma_6^- \rightarrow \Gamma_{12}$. Indeed, the second peak does split into two components at low temperature. It seems unlikely that the fourth peak appearing at low temperature (7.35 eV) could be a SO-split exciton associated with Γ_1 or Γ_{12} because it is so strongly temperature dependent, in contrast to the first three peaks. In KBr the SO splitting of the $\text{Br}^-(4p)$ valence band is 0.51 eV. This splitting is more closely maintained in CsBr if the second and third peaks at low temperature are assigned to $\Gamma_8^- \rightarrow \Gamma_{12}$ and $\Gamma_6^- \rightarrow \Gamma_1$ excitons, respectively (see Table III). The strongly temperature-sensitive fourth peak at 7.35 eV and the shoulder at 7.87 eV may also be SO-split structures. This assignment also gives a larger splitting of the Γ_{12} excitons than of the Γ_1 excitons, as in CsCl .

The broad structures (centered at 11 and 10 eV in CsCl and CsBr) as well as the strong peak just below them (9.12 and 8.51 eV, respectively) are similar in the two crystals. While the assignment of these peaks is uncertain, their large width indicates that they are associated with interband

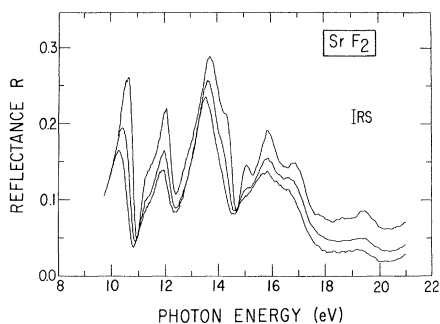


FIG. 10. Reflectance spectra of SrF_2 in the valence excitation region, $RS=0.0175$.

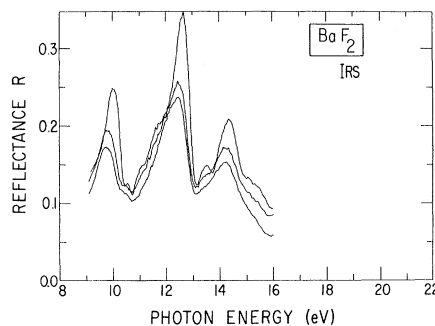


FIG. 11. Reflectance spectra of BaF_2 in the valence excitation region. The curves are not shown above 16 eV, where core excitations dominate the spectra, $RS=0.0175$.

transitions, not excitons.

VII. CORE EXCITONS

The sharp peaks which characterize region II of the reflectance spectra (Fig. 5) are believed to be exciton absorption bands involving electrons in the p core levels which form the outer shell of the $+$ ions. Accordingly, crystals with the same alkali or alkaline-earth ion have similar reflectance spectra in region II. In most cases the strong core exciton peaks can be grouped into SO-split pairs by their observed temperature dependence and by the SO splitting of the initial (core) states, known from atomic x-ray data⁶² (Table VI). Furthermore, from theoretical models of the conduction bands of the crystals, it is possible to identify the core excitons with the electronic states in the Brillouin zone from which they are formed. It should be noted, however, that for the most part the correlations and assignments of structure in region II are independent of whether these features are excitons or simply structure in the interband density of states. Nevertheless, the present evidence favors the exciton interpretation (discussed more thoroughly in Sec. IX).

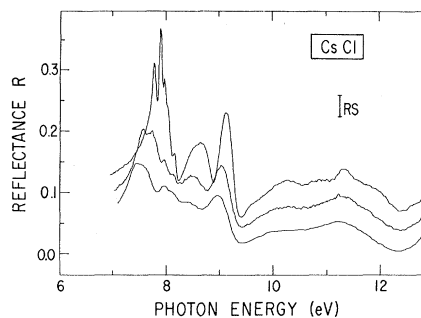


FIG. 12. Reflectance spectra of CsCl in the valence excitation region, $RS=0.035$.

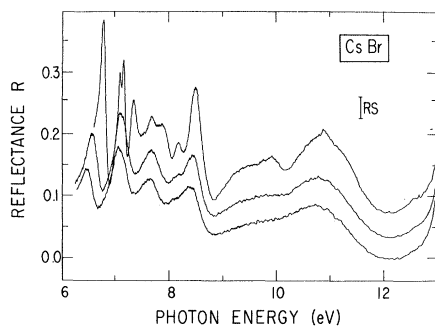


FIG. 13. Reflectance spectra of CsBr in the valence excitation region, $RS=0.035$.

A. RbCl

The reflectance spectra of RbCl in the core exciton region are shown in Fig. 14. Five sharp peaks appear below the start of region III (interband transitions of core electrons) at 18.3 eV. According to the schematic band structure shown in Fig. 2, one expects to observe core excitons associated with transitions to Γ_1 , followed at somewhat higher energy by excitons related to states at X_3 . In each case, two excitons should be observed due to the SO splitting of the flat core levels [the atomic Rb($4p$) splitting is 0.8 eV].⁶² The temperature-dependent reflectance spectra of RbCl (Fig. 14) show that peaks A_1 and A_2 have similar shifts in energy with temperature (see Table V). The negative temperature shifts (to higher energy upon cooling) which they display is common in ionic crystals. The position of peak A_1' is nearly independent of temperature. In contrast, peaks B_1 and B_2 have positive temperature shifts (to lower energy at lower temperature). Temperature shifts of core excitons are expected to arise primarily from changes in the energy of the associated conduction-band states. Hence A_1 and A_2 are identified as the Γ core excitons [$\text{Rb}^+(4p) \rightarrow \Gamma_1$] while B_1 and B_2 are considered the X excitons [$\text{Rb}^+(4p) \rightarrow X_3$].^{22,33,65} The peak A_1' may be an excited state of the A_1 exciton.⁶⁶

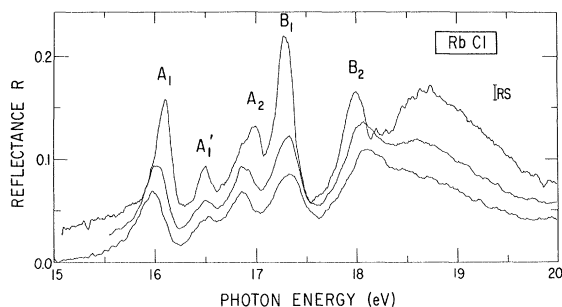


FIG. 14. Reflectance spectra of RbCl in the core exciton region, $RS=0.014$.

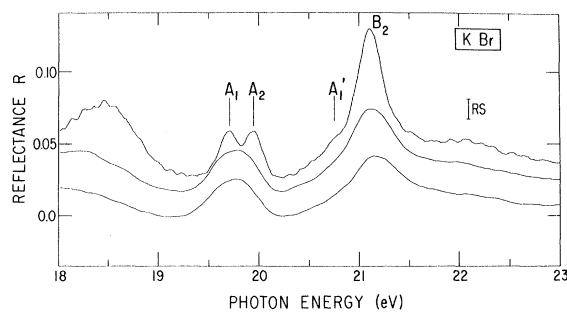


FIG. 15. Reflectance spectra of KBr in the core excitation region, $RS=0.014$.

The Γ and X core exciton pairs in RbCl each have approximately the 2:1 intensity ratio expected for the $j = \frac{3}{2} : j = \frac{1}{2}$ components of the SO-split core level. Because of the rather large SO splitting, exchange effects (which can alter the ratio) should be small.⁶³ However, it is puzzling that the SO splitting of the Γ excitons (0.89 ± 0.03 eV) is different from that of the X excitons (0.73 ± 0.03 eV), since exchange effects (which might be different for Γ and X excitons) should not alter the SO splitting of core states.⁶³

B. KBr and KCl

Two sharp core exciton peaks appear in region II of KBr and KCl, as shown in Figs. 15 and 16. At low temperature the lower-lying peak splits into a doublet, which has been observed in electron energy-loss measurements⁶⁷ and also recently by other workers in reflectance.^{33,43} The separation between A_1 and A_2 is approximately 0.27 eV, the SO splitting of the $\text{K}^+(3p)$ atomic level.⁶² Hence A_1 and A_2 are identified as the SO-split $j = \frac{3}{2}$ and $j = \frac{1}{2}$ core excitons associated with $\text{K}^+(3p) \rightarrow \Gamma_1$, respectively.^{43,67} A 2:1 intensity ratio for these peaks is not observed in either KBr or KCl. In KBr the doublet is fairly isolated from other structures (see Figs. 5 and 15). We believe²² that the 1:1 intensity ratio in KBr arises from the effects of exchange interaction,⁶³ which are large due to the small SO-splitting parameter. An exchange splitting $\Delta \approx 0.1$ eV for a doublet with SO splitting $\lambda = 0.27$ eV will produce the observed intensity ratio of 1:1. The strong valence excitation structure at 18.5 eV in KBr shifts to 19.5 eV in KCl and overlaps A_1 considerably (compare Figs. 15 and 16). The degeneracy of A_1 with strong valence excitations in KCl may enhance the rate at which the A_1 exciton decays by nonradiative processes into interband excitations of valence electrons. Consequently, lifetime broadening of A_1 in KCl suppresses its relative magnitude even further.

The B_2 peak is considered^{22,37,38,58,67} a core exciton associated with the minimum at X_3 of the d -

like conduction bands. It has a positive temperature shift. The lack of a SO splitting of B_2 has been attributed to a shorter lifetime resulting from energy degeneracy with the conduction band.⁵⁸ However, this explanation seems unlikely because the width of B_2 is approximately equal to that of A_1 or A_2 . If one were to broaden the peaks of a doublet like A_1 and A_2 in KBr until the splitting disappears (to account for shorter lifetimes), the resulting structure would be at least three times broader than the observed B_2 .

As an alternative^{22,33} we suggest that exchange interaction⁶³ may suppress the lower component ($j = \frac{3}{2}$) of the SO-split X_3 excitons so that only the higher component B_2 ($j = \frac{1}{2}$) is observed. For negligible crystal potential (appropriate for core states), the intensity ratio of the $j = \frac{3}{2} : j = \frac{1}{2}$ components changes with Δ/λ (exchange parameter/SO parameter) in the same fashion at X as at Γ . Therefore, the exchange parameter Δ must be larger for core excitons at X than at Γ . For a doublet SO split by 0.27 eV, an exchange splitting $\Delta = 0.25$ eV will produce a 1:4 intensity ratio, so that the lower peak is very difficult to observe.

The A_1' shoulder appears clearly in KCl and is faintly suggested in KBr by the change in slope of the reflectance at 20.8 eV. This shoulder is too far away from B_2 to be the missing B_1 peak. A_1' may be either an excited state of the A_1 exciton or the $K^+(3p) \rightarrow \Gamma_1$ core interband edge. The ESCA data⁶⁰ support the latter interpretation (Sec. V). It is also conceivable that A_1' is an excitation of the Cl^- valence band, corresponding to the shoulder in RbCl at 20.8 eV (see Fig. 5). In any case, the A_1' shoulder is probably too weak to cause complete suppression of the expected B_1 exciton by lifetime broadening (an even stronger peak at 19.5 eV in KCl does not fully suppress A_1).

C. CsCl and CsBr

The reflectance spectra of CsCl and CsBr in the region of core excitations are shown in Figs. 17 and 18. Core excitons are believed to dominate the

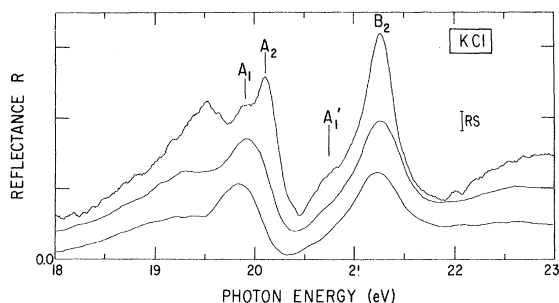


FIG. 16. Reflectance spectra of KCl in the core excitation region, $RS=0.014$.

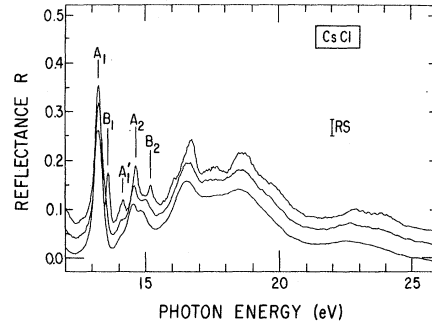


FIG. 17. Reflectance spectra of CsCl in the region of core excitations, $RS=0.035$.

spectra between 13 and 16 eV (region II), while interband transitions produce the features at higher energy.

Five sharp core exciton peaks occur in CsCl. The first exciton A_1 is extremely strong—as strong as the excitons at the fundamental absorption edge (see Fig. 5). The SO splitting of the $Cs(5p)$ atomic state is 1.7 eV.⁶² Peaks A_1 and A_2 , separated by 1.39 eV, have roughly a 2:1 intensity ratio. Peaks B_1 and B_2 have similar ratio and are separated by 1.62 eV. The temperature shifts of B_1 and B_2 are noticeably larger than those of A_1 and A_2 . B_1 appears separate from A_1 only at low temperature. The A_1 and A_2 excitons are assigned to $Cs^+(5p) \rightarrow \Gamma_1$, while B_1 and B_2 are associated with $Cs^+(5p) \rightarrow \Gamma_{12}$ (see Fig. 4). A_1' may be an excited state of the A_1 exciton.

Since the core exciton spectra of CsBr are very similar to those of CsCl, the assignment of the labeled peaks in Fig. 18 is the same. However, even at low temperature the B_1 exciton is nearly degenerate with A_1 , appearing almost as a shoulder. Hence the energy separation between Γ_1 and Γ_{12} must be smaller in CsBr than in CsCl. At low temperature, a shoulder appears on the low-energy side of B_2 in CsBr. The temperature shift of the energies of the Γ_{12} excitons (B_1 and B_2) is larger in

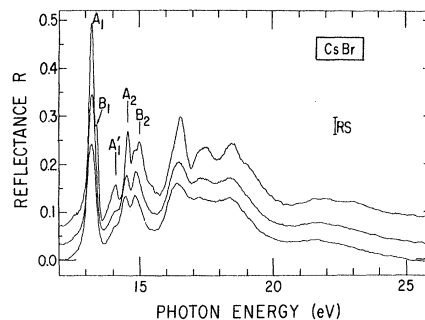


FIG. 18. Reflectance spectra of CsBr in the region of core excitations, $RS=0.035$.

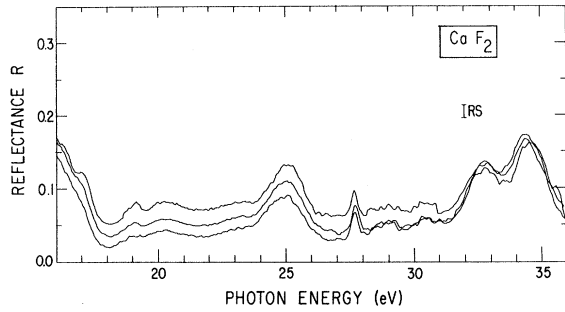


FIG. 19. Reflectance spectra of CaF_2 in the region of core excitations, $RS=0.0175$.

CsCl than in CsBr . Finally, in both crystals the $\text{Cs}^+(5p)$ SO splitting determined from the separation of the Γ_1 excitons (1.38 eV) is smaller than that obtained from the separation of the Γ_{12} excitons (1.61 eV); this was also observed for the SO splitting of the valence band as measured by the valence excitons (see Sec. VI).

D. CaF_2 , SrF_2 , and BaF_2

The reflectance spectra of CaF_2 , SrF_2 , and BaF_2 in the core excitation region are shown in Figs. 19–21. The SO splitting of the $\text{Ba}(5p)$ atomic state is 2.0 eV, while for $\text{Sr}(4p)$ and $\text{Ca}(3p)$ the splitting is negligible.⁶² In CaF_2 only one sharp exciton peak appears, at 27.7 eV. This is considered to be the $\text{Ca}^{++}(3p) - \Gamma_1$ exciton. The large width of the 25.1-eV peak, as well as the atomic x-ray data (Sec. V), indicate that it is not associated with the $\text{Ca}^{++}(3p)$ core level. It has been suggested that the 25.1-eV peak arises from transitions to high-lying conduction band states from either the $\text{F}^-(2s)$ core level⁴² or from the second set of valence bands (associated with Γ'_{25} in Fig. 3).⁴⁷

Because the $\text{Sr}(4p)$ SO splitting is negligible, peaks A and B in Fig. 20 are most likely the core excitons associated with the minima of the s -like conduction band at Γ_1 and of the d -like conduction band at X_3 , respectively (see Fig. 3). The X exciton (B) is stronger than the Γ exciton (A), as in

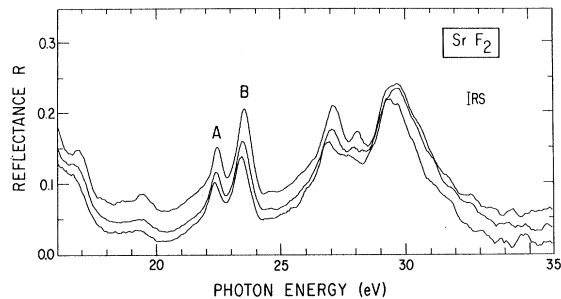


FIG. 20. Reflectance spectra of SrF_2 in the region of core excitations, $RS=0.0175$.

KCl and KBr where a similar conduction-band structure is expected and the SO splitting of the core level is also small.

In BaF_2 the 2.0-eV SO splitting of the $\text{Ba}(5p)$ core suggests that A_1 and A_2 are the SO split excitons associated with Γ_1 , while the B_1 and B_2 excitons involve the d -like conduction bands at X_3 . However, for both pairs the intensity ratio of the components is very different from the expected 2:1 value. The shoulder which appears at low temperature on the high-energy side of A_1 is also unexplained.

The reflectance peaks observed in region II display many of the general characteristics one would expect for core excitons. They are as sharp as the valence exciton peaks. The monochromator resolution does not allow an accurate assessment of the temperature dependence of the exciton widths.⁶⁸ However, strong temperature dependence of the core excitons, a result of the strong electron-lattice interaction in ionic crystals,⁶⁹ is seen in the enhancement of the exciton peaks at low temperature. Furthermore, the observed positions, magnitudes, and temperature shifts allow a grouping of SO-split core exciton pairs and a reasonably consistent identification in terms of the electronic band structure.

However, the assignments given for the core excitons leave some details unexplained. The observed SO splittings of different core excitons (e.g., Γ_1 and X_3) in the same crystal are not identical, even though exchange effects on the splittings of core excitons should be negligible.⁶³ In CsCl and CsBr the separation of the Γ_1 and Γ_{12} conduction-band states (Fig. 4) is not the same when determined from core rather than valence excitons. The temperature shifts of the SO-split components of the core excitons are not always equal (e.g., A_1 and A_2 in CsCl), nor do the lowest and excited states of the same core exciton (e.g., A_1 and A'_1 in RbCl) have the same temperature shifts. It is plausible that these effects arise from the complexity of the exciton structure. Because of the short radius of the exciton, band states from a sizable portion of the

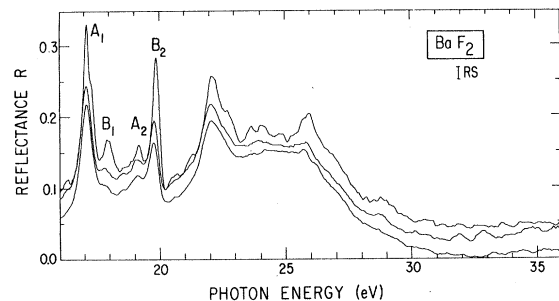


FIG. 21. Reflectance spectra of BaF_2 in the region of core excitations, $RS=0.0175$.

Brillouin zone are needed to make up the exciton wave function (e.g., of order $\frac{1}{4}$ the zone radius or more for valence excitons in KCl).¹⁶ The spatial dependence of the dielectric constant in (1) may produce a sensitivity of the exciton energy levels to the instantaneous position of the ions. As a result, exciton binding energies may be temperature dependent. Finally, localization of the core hole may produce different screening and different binding energies for the core and valence excitons.

VIII. INTERBAND TRANSITIONS OF CORE ELECTRONS

The reflectance spectra in region III (Fig. 5) are dominated by structures considerably broader than the sharp core exciton peaks in region II. These broader features, lying at higher energy than the core excitons, arise from interband transitions of core electrons. Since the core bands are flat, the shape of the core interband spectra is determined by the wave functions and density of states of the conduction bands. In contrast to the exciton region, the interband spectra in region III show no clear evidence of the SO splitting of the initial (core) states. This may occur because (as in the valence interband region) a considerable number of different interband transitions contribute to the observed reflectance and mask the duplication of structure produced by SO splitting.

In the core interband region, the reflectance spectra are similar for crystals having a common crystal structure. As seen in Fig. 5, the NaCl-type crystals (KBr, KCl, and RbCl) show a series of fairly weak ($\Delta R \approx 4-7\%$), broad peaks rather evenly spaced in energy (about 3 eV apart). In contrast, the CsCl-type crystals (CsCl and CsBr)⁷⁰ and the CaF₂-type crystals (CaF₂, SrF₂, and BaF₂) have remarkably similar spectra in region III: A stronger ($\Delta R \approx 11\%$) doublet about 4 eV wide dominates the spectrum, and at low temperature shoulders appear on both sides of the doublet, as well as a weak peak in its center. Figure 1 shows that, in both the CaF₂- and the CsCl-type crystals, the + ions have an eightfold coordination of nearest neighbors (- ions). This is in contrast to the sixfold coordination of nearest neighbors which the + ions in the NaCl-type crystals have. Thus the shape of the core interband spectra appear to be determined in large part by the spatial coordination of the + ions. We expect this coordination to be important because the excited states of the + ions form the basis for the lowest 6 eV or so of the conduction bands. There is no correspondence of the spectra with the nearest-neighbor coordination of the - ion. Furthermore, the spectra are not correlated with the shape of the Brillouin zone; the CaF₂- and NaCl-type crystals have the same Brillouin zone (for the fcc lattice), whereas the CsCl-type crystals have a different Brillouin zone (for a simple cubic lat-

tice).⁷¹

The strong dependence of the core interband structures on the nearest-neighbor coordination of the + ions is plausible in view of the nature of the electronic states in the lowest 6 eV or so of the conduction bands. As explained in Sec. II, these bands originate from the excited *s* and *d* states of the + ions and maintain a strong atomic character in the crystal. Broadening of the excited levels of the ions into conduction bands is produced by the overlap of free-ion wave functions from different ions. Nearest neighbors (the - ions) are likely to make the strongest contribution to the broadening of the + ion levels in the crystal. Hence the nearest-neighbor coordination of the + ions will have a strong, perhaps even dominant, effect on the conduction-band states which determine the shape of the reflectance in the core interband region.

The features of the reflectance spectra in region III are most likely caused by transitions to *d*-like conduction-band states, which dominate the density of states above the *s*-like conduction-band minimum.⁷⁻¹⁵ It is interesting to note that in CsCl and CsBr a fairly broad structure, resembling the core interband doublet, appears in the valence excitation region near 11 eV. The valence-band structure in the Cs halides may be such that the same conduction-band states are important for both the valence and core interband spectra. No comparable similarities between valence and core interband spectra appear in the other crystals.

IX. EXISTENCE OF CORE EXCITONS

A fundamental question in the far-ultraviolet and soft x-ray spectroscopy of ionic crystals is the strength of core exciton effects in the absorption spectrum. In regard to the present experiment, one can ask more specifically if the sharp reflectance peaks near the core onset represent exciton absorption rather than simply structure in the interband density of states. The Wannier model predicts that strong excitons should be present in ionic crystals (as certainly occurs in the valence excitation region). Furthermore, like the valence excitons, the anticipated core excitons involve holes in the outer electronic shell of the ions. Therefore it is natural to assume that core excitons dominate the optical spectrum at and just above the core onset, while interband transitions are more important at higher energies.

The experimental results presented here tend to support (but do not prove) this assumption. The reflectance peaks in region II (Fig. 5) are as sharp as valence excitons, in marked contrast to the broader features in region III. In region II the spectra are characteristic only of the + ions and seem therefore to represent excitations of these ions alone, whereas in region III the shape of the

spectra is primarily determined by the crystal structure and therefore depends strongly on both + and - ions. The peaks in region II are sufficiently sharp and simple that SO-splitting effects can be observed, which is not the case in region III.

Sharp peaks like those attributed to core excitons also appear in the photoemissive quantum yield of the Rb halides,^{59,72} and the K halides,^{58,73-75} and in the yield due to Na⁺(2*p*) core excitations in NaCl.⁷⁶ The peaks in the photocurrent persist even for large retarding potentials (6-11 eV).^{58,59,75,76} This is surprising⁷⁷ because for reflectance peaks near the core onset the energy of the excited core electron lies below the vacuum level, regardless of whether the peak arises from excitonic or interband transitions. Furthermore, for core excitons the near-infinite effective mass of the core hole makes it difficult for the electron, bound to the hole, to reach the surface of the sample and contribute to the photoemissive current. We also note that when the broad background is subtracted from the yield curves to compare with optical absorption, it appears that in photoemission the sharp peaks in region II are somewhat suppressed compared to the higher-energy structures in region III.

It has been suggested^{58,59,72-76} that the core exciton peaks in region II appear in photoemission with large retarding potentials because nonradiative decay of these excitons produces electrons having large kinetic energies (of order 15 eV or more). Since not all of the core excitons are expected to decay nonradiatively, the peaks in region II should appear somewhat weaker than do the structures in region III, where interband transitions produce electrons at energies above the vacuum level; as already noted, this seems to be the case. However, we also note that the presence of nonradiative decay processes for the sharp structures in region II does not directly prove that these peaks are core excitons. Instead, the exciton decay processes must be examined in detail.

The basic decay modes of the exciton are depicted in Fig. 22. Direct radiative recombination, in which a photon is emitted, is shown in Fig. 22(a). This occurs for any exciton, valence or core, which is optically excited. At finite temperature, scattering by phonons produces an additional contribution to the observed width.

If the exciton energy is degenerate with the conduction-band continuum, then the exciton (valence or core) can decay by the configuration interaction (CI) process shown in Fig. 22(b). The Coulomb interaction which arises between electron and hole in the excited state produces matrix elements of the form⁷⁸

$$V = \left\langle \psi_{kc}(\mathbf{r}_e) \psi_{kv}(\mathbf{r}_h) \left| \frac{e^2}{|\mathbf{r}_e - \mathbf{r}_h|} \right| \phi(\mathbf{r}_e - \mathbf{r}_h) \right\rangle, \quad (5)$$

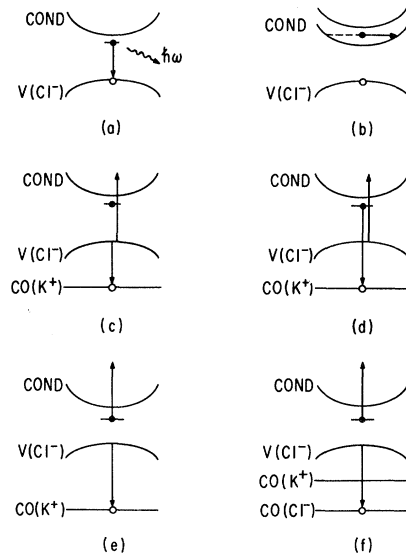


FIG. 22. Basic exciton decay modes. The electron and hole in the initial (exciton) state are designated by solid and open circles, respectively, while arrows signify electron transitions during the decay process. Conduction, valence, and core bands are indicated by COND, V, and CO, respectively. The ions on which the valence and core bands are localized are noted in parentheses, using KCl as an example. Both valence and core excitons can decay by radiative recombination (a) or by configuration interaction mixing with the continuum (b). In (c), Auger decay results in two electron-hole pairs. Processes (d) and (e) are indistinguishable modes of CI decay in which the states of both the electron and the hole change. The decay of the soft x-ray exciton in (f) is similar to that in (e) except that it can occur within a single ion.

where ϕ is the exciton wave function, r_e and r_h are the electron and hole positions, and ψ_{kc} and ψ_{kv} are their final-state wave functions in the conduction and valence bands. Thus the final-state Coulomb interaction, neglected in the one-electron band-structure picture, mixes the exciton state with states of the free-electron-hole pair having the same energy. Interference between the bound (exciton) and free (interband) states of the electron and hole can produce antiresonance characteristics⁷⁹ in the observed exciton line shapes.^{18,19} If the CI decay rate is sufficiently large [i. e., the mixing in (5) is strong], the exciton peak may be so broadened that no exciton is observed; instead, the oscillator strength is concentrated in interband absorption.

The core excitation spectra of the crystals studied here strongly suggest the presence of two sets of core excitons, one from *s*-like and one from *d*-like conduction bands, at energies below the region of core interband transitions. Likewise, two corresponding sets of excitons are observed in the valence region. This can be partially understood on the basis of approximate selection rules for non-

radiative decay by CI. Since the exciton wave function ϕ is composed of electron and hole states which are made up from band states, the matrix element (5) can be written in a more general form which describes any simultaneous transition of electron and hole as

$$V = \left\langle \psi_e^f(r_e) \psi_h^f(r_h) \left| \frac{e^2}{|r_e - r_h|} \right| \psi_e^i(r_e) \psi_h^i(r_h) \right\rangle, \quad (6)$$

where the subscripts e and h denote electron and hole functions, and the superscripts i and f represent initial and final states. Since the perturbation in (6) is part of the real many-body Hamiltonian, $V=0$ unless the initial and final electron-hole states have the same symmetry.⁸⁰ The band states largely retain the angular momentum character of the ionic states from which they originate. Since the hole wave function is unchanged in the (valence or core) exciton decay process shown in Fig. 22(b), strong CI can occur only if the electron states ψ_e^i (exciton) and ψ_e^f (band) have similar angular momentum symmetry. The first two sets of excitons, associated with s - and d -like conduction bands, lie below the conduction-band continua of the same s or d symmetry and therefore cannot be greatly broadened by CI. In contrast, nonradiative decay by CI should strongly broaden and suppress a third possible set of excitons associated with d -like states (e. g., near Γ'_{25} in Fig. 2), because these excitons would be degenerate with d -like band states (e. g., along the ΓX line). Accordingly, interband transitions are expected to dominate the absorption associated with states near Γ'_{25} , as seems to be the case (see Sec. VI).

Blechs Schmidt *et al.*⁵⁸ and Haensel *et al.*⁷⁶ have considered both the Auger and direct recombination processes, shown in Figs. 22(c) and 22(d), respectively, as possible nonradiative decay modes to explain the presence of the sharp core excitation peaks in their photoemission results. From analyzing the kinetic energy of the photoelectron, they showed that the Auger process is not important in comparison with recombination. The direct recombination process is induced by CI according to (6), but the hole as well as the electron state is changed. Figure 22(e) shows an alternate description of this process equivalent (having the same matrix element) to that in Fig. 22(d).

Nonradiative decay by Coulombic CI can occur for interband excitations of core electrons as well as for core excitons. The matrix elements (6) corresponding to the two cases differ only in the initial electron state $\psi_e^i(r_e)$, which is localized near the hole for the core exciton but extended (in a Bloch state) for the interband transition. If dynamical effects accompanying the decay process are disregarded, the Coulomb interaction energy $e^2/|r_e - r_h|$ will be much larger when the electron is localized

near the hole than when it is in an extended Bloch state. Accordingly, we expect the matrix element (6) to be much larger (perhaps several orders of magnitude) for decay of the core exciton than for decay of a core interband excitation. The magnitudes of the sharp peaks in the photoemissive yield are of order several percent per absorbed photon above the background.^{59,72,74,75} This cannot be explained by the low nonradiative decay rate expected for core interband excitations, so that by this rough analysis, core excitons must produce the sharp peaks which are observed just above the core onset in photoemission as well as in reflectance and absorption.

Although nonradiative decay of core excitons by CI appears to occur in the far ultraviolet, the rather low quantum yield of the core exciton peaks indicates that radiative decay remains the dominant and therefore the faster process.⁸¹ As seen in Figs. 22(d) and 22(e), the nonradiative decay process requires an electron to travel about one interionic spacing (from the $-$ to the $+$ ion) to recombine with the core hole. The maximum band velocity of a valence electron having effective mass $2m_0$ is about 3×10^7 cm/sec, so that the decay process cannot occur in less than 10^{-15} sec. Thus, lifetime broadening must be less than 1 eV for core excitons having holes in the outer shell of the $+$ ions. In fact, the observed core excitons have widths ≤ 0.2 eV, so that nonradiative lifetime broadening may be less than 0.05 eV.

In contrast, core excitons in the soft x-ray region do not require interionic electron transfer for nonradiative decay. As seen in Fig. 22(f), the core hole lies in the inner shell of the ions, so that an electron from the outer shell of the same ion can rapidly recombine with the hole. Thus lifetime broadening by CI and possibly by Auger processes may be so severe that excitons are not observed. The role of excitons in the soft x-ray spectra of ionic crystals has received considerable attention.⁸²⁻⁸⁷ Recently, calculations of the soft x-ray absorption spectra of ionic crystals^{82,87,88} have been found to give good agreement with experiment without the introduction of bound states of the electron-hole pair (excitons). Thus it appears that severe lifetime broadening may suppress excitons in the soft x-ray region, but not in the far-ultraviolet portion of the spectrum studied in the present work.

X. TEMPERATURE DEPENDENCE AND BAND STRUCTURE

The shift of exciton peaks with temperature is usually attributed to the temperature dependence of the associated interband edge, although it is possible (see Sec. II) that the exciton binding energies have a weak temperature dependence. Since the energies of core levels are insensitive to the

crystal potential (and therefore temperature independent), shifts of the core excitons reflect primarily the temperature dependence of the conduction-band states. Therefore, the data in Table V shows that the *s*-like conduction-band states (near Γ_1) are considerably less sensitive to temperature than are *d*-like states (near X_3 in the fcc crystals and near Γ_{12} in the simple cubic crystals). In the alkali halides, the conduction-band minima at Γ (either Γ_1 or Γ_{12}) shift to higher energy upon cooling, while the states near X_3 move to lower energy at lower temperature.⁶⁵ A similar positive temperature shift of *X* excitons has been observed in the $\text{Na}^+(2p)$ absorption spectra.⁸⁹

Many structures throughout the reflectance spectra are greatly sharpened and enhanced at low temperature (see Fig. 5). While such effects are not unusual for excitons,^{16,69} the temperature sensitivity of structures associated with both valence and core interband transitions is remarkably large (in Fig. 5 see, e. g., KCl at 14 and 19.6 eV, RbCl at 18.8 eV, CsCl at 11.3 eV, CsBr at 18.6 eV, CaF_2 at 14.4 eV, SrF_2 at 28.2 eV, and BaF_2 at 26.0 eV). The temperature dependence observed here is even stronger than that observed by Bauer and Spicer⁹⁰ in photoemission from the Ag halides. They showed that the strong broadening of photoemission structures at finite temperature can be attributed to a smearing of the valence-state eigenvalues by the lattice vibrations. The electronic energies depend on the position of the ions through the deformation-potential coupling. The time average of the random lattice vibrations at finite temperature gives a smearing of the ionic positions, which creates a corresponding broadening of the electronic energies. Bauer and Spicer⁹⁰ found that at room temperature the rms displacement of the ions in AgCl is about 10% of the interionic separation. As a result, the energy of the L'_3 valence state varies over a 1.1 eV range. This broadening of electronic energies with temperature accounts for the strong sharpening and enhancement of structures observed at low temperature.

The crystals studied here are expected to have ionic displacements with temperature comparable to those in AgCl. Furthermore, the interband deformation potentials of the alkali halides^{25,27} are roughly half as large as the 5.5-eV deformation potential of the L'_3 valence level in AgCl.⁹⁰ Consequently, a strong temperature dependence of interband reflectance structures, as observed here, is expected as a result of the broadening of electron energy levels by lattice vibrations. However, since the core bands are insensitive to the lattice, the temperature dependence of core interband structures implies that conduction-band states in ionic crystals must also be sensitive to lattice vibrations (i. e., they must have deformation potentials com-

parable to those of the valence bands). This is plausible because the conduction-band states retain considerable ionic character and localization and depend strongly on the overlap of wave functions from neighboring ions.

Deformation potentials in ionic crystals are no larger than those in other solids. In semiconductors,^{91,92} e. g., deformation potentials are at least as large as in ionic crystals. Therefore, the striking temperature dependence observed in ionic crystals cannot be a consequence of exceptionally large deformation potentials (or large ionic displacements, for that matter). Instead, it must result more from the fact that the low-temperature optical spectra of ionic crystals, in contrast to other solids, contain structures sufficiently sharp that the broadening by lattice vibrations at higher temperature can be observed. Furthermore, because the exciton energies are tied to the interband edges, it is not surprising that the exciton bands (inherently narrow) also display strong temperature dependence.

XI. CONCLUSION

Synchrotron radiation provides an excellent opportunity to investigate the optical properties of ionic crystals. We have measured the reflectance spectra of a number of these solids over a broad range of energy (6 to 36 eV) and temperature (90 to 400 °K). In the higher-energy region where excitations of core electrons in the outer shell of the + ions dominate, the spectra indicate a natural division into two parts: Just above the core onset, sharp peaks due to core excitons appear, while at somewhat higher energies, considerably broader structures arise from interband transitions of core electrons.

The sharp core exciton peaks can be correlated with the identity of the + ion and assigned to transitions in the Brillouin zone by their temperature dependence and SO splittings. Because of the high energy of excitation, the core excitons can undergo nonradiative decay by Auger as well as by CI processes involving the valence bands. The presence of the sharp peaks in photoemission is evidence that these decay processes, which yield electrons with large kinetic energies, occur in the ionic crystals.^{58,59,72-76} In fact CI has been shown to be much more important in the far ultraviolet than the Auger processes.^{58,76} Because of the smaller electron-hole separation in the exciton state, it is suggested that the Coulombic CI matrix element is much larger for the decay of core excitons than for core interband transitions. Therefore, the size of the sharp peaks in photoemission (quantum yield of order several percent) is a strong indication that the peaks must be caused by excitons. Furthermore, it is shown that lifetime broadening of the

core excitons observed here cannot be large enough to completely suppress the excitons, because the hole lies in the outer electronic shell of the ions. In contrast, excitons in the soft x-ray region involve inner-shell holes, so that lifetime broadening may be much more severe and may account for the observation^{82, 87, 88} that excitons (the bound states of the electron-hole pair) are not required to explain the soft x-ray absorption spectra of ionic crystals.

The broader core excitation structures at higher energy appear to arise from interband transitions. The shapes of these features are correlated with the nearest-neighbor coordination of the + ion. This crystal structure effect underscores the fact that the conduction-band wave functions largely retain the character of excited states of the + ions, broadened by nearest-neighbor overlap.

As shown previously for the silver halides, vibrations of the lattice in the ionic crystals modulate valence-band energies through the deformation-potential coupling, so that sharp structures in the spectrum of valence interband excitations are greatly broadened at elevated temperatures. The strong temperature dependence of core interband features suggests that lattice vibrations have a similar effect on states in the conduction bands. Furthermore, since exciton levels follow the conduction-band energies, strong temperature dependence of the excitons is also observed.

This temperature-broadening process appears not to be restricted to ionic crystals, because their deformation potentials and ionic displacements are not noticeably larger than those in other solids. However, the broadening can be observed only in solids, like the ionic crystals, where the natural widths of the structures are not much larger than the contribution from thermal broadening. Therefore, the remarkable feature of the ionic crystals is not so much their temperature dependence, as

it is the inherent sharpness of their optical spectra at low temperature.

The dramatic sharpness of the ionic crystal spectra is primarily a consequence of the strong ionic character of the crystalline eigenstates. Because both the + and - ions have closed outer electronic shells, the charge densities of the filled states (valence as well as core) are considerably localized. The resulting valence bands are of order 0.75 eV wide.⁸⁻¹⁵ Since the lower-lying conduction bands retain the character of the ionic states from which they are formed, rather sharp peaks (of order 1 eV wide) also appear in the conduction band density of states.^{12, 82, 87, 88} Furthermore, the strong localization of the electronic charge density weakens the screening of the Coulomb interaction between the excited electron and the hole. As a result, portions of the joint density of states observed in interband transitions can be further sharpened,^{17, 20, 21} while additional strong peaks appear due to the formation of excitons.

ACKNOWLEDGMENTS

It is a great pleasure for me to thank Professor H. Fritzsche for his invaluable guidance and assistance, his sincere encouragement, and his enthusiastic support during the course of this research. I am also very grateful to J. Freeouf and K. Murase for their close cooperation and substantial help in many phases of this work, and to U. Gerhardt for his numerous contributions in the early stages of our project at the storage ring. I thank also J. Sak, T. Bergstresser, and M. H. Cohen for enlightening discussions about these results. Finally, I am very pleased to acknowledge the complete cooperation and genuine encouragement of the staff of the University of Wisconsin Physical Science Laboratory, especially E. M. Rowe, C. H. Pruett, and R. Otte.

*Research sponsored by the Air Force Office of Scientific Research, Office of Aerospace Research, U. S. A. F., under Contract Nos. F44620-71-C-0025 and F44620-70-C-0029. The U. S. Government is authorized to reproduce and distribute reprints for Governmental purposes notwithstanding any copyright notation hereon. I have also benefited from support of Materials Sciences by the Advanced Research Projects Agency at The University of Chicago.

†Submitted in partial fulfillment of the requirements for the Ph.D. degree at The University of Chicago.

‡Fannie and John Hertz Foundation Fellow.

§Present address: Department of Physics, Brown University, Providence, R.I. 02912.

¹R. Hilsch and R. W. Pohl, *Z. Physik* **59**, 812 (1930).

²For a comprehensive review of the experimental aspects of vacuum-ultraviolet spectroscopy, see J. A. R. Samson, *Techniques of Vacuum Ultraviolet Spectroscopy* (Wiley, New York, 1967).

³R. P. Godwin, *Springer Tracts Mod. Phys.* **51**, 1

(1969).

⁴E. M. Rowe, R. A. Otte, C. H. Pruett, and J. D. Steben, *Trans. IEEE Nucl. Sci.* **NS-16**, 159 (1969).

⁵G. W. Rubloff, H. Fritzsche, U. Gerhardt, and J. Freeouf, *Rev. Sci. Instr.* **42**, 1507 (1971).

⁶L. P. Howland, *Phys. Rev.* **109**, 1927 (1958).

⁷S. Oyama and T. Miyakawa, *J. Phys. Soc. Japan* **21**, 868 (1966).

⁸Y. Onodera, M. Okazaki, and T. Inui, *J. Phys. Soc. Japan* **21**, 2229 (1966).

⁹P. D. DeCicco, *Phys. Rev.* **153**, 931 (1967).

¹⁰A. B. Kunz, *Phys. Status Solidi* **29**, 115 (1968).

¹¹A. B. Kunz, *Phys. Rev.* **175**, 1147 (1968).

¹²C. Y. Fong and M. L. Cohen, *Phys. Rev.* **185**, 1168 (1969).

¹³L. J. Page and E. H. Hygh, *Phys. Rev. B* **1**, 3472 (1970).

¹⁴Y. Onodera, *J. Phys. Soc. Japan* **25**, 469 (1968).

¹⁵U. Rössler, *Phys. Status Solidi* **34**, 207 (1969).

¹⁶A detailed discussion and review of the exciton problem

is given in R. S. Knox, *Theory of Excitons*, Suppl. 5 of *Solid State Physics* (Academic, New York, 1963).

¹⁷Y. Toyozawa, M. Inoue, T. Inui, M. Okazaki, and E. Hanamura, *J. Phys. Soc. Japan Suppl.* **21**, 133 (1966).

¹⁸J. C. Phillips, *Phys. Rev. Letters* **12**, 447 (1964).

¹⁹K. P. Jain, *Phys. Rev.* **139**, A544 (1965).

²⁰B. Velicky and J. Sak, *Phys. Status Solidi* **16**, 147 (1966).

²¹E. O. Kane, *Phys. Rev.* **180**, 852 (1969).

²²G. W. Rubloff, J. Freeouf, H. Fritzsche, and K. Murase, *Phys. Rev. Letters* **26**, 1317 (1971).

²³J. Eby, K. Teegarden, and D. Dutton, *Phys. Rev.* **128**, 1656 (1962).

²⁴K. Teegarden and G. Baldini, *Phys. Rev.* **155**, 896 (1967).

²⁵D. W. Lynch and A. D. Brothers, *Phys. Rev. Letters* **21**, 689 (1968).

²⁶G. Baldini and B. Bosacchi, *Phys. Rev.* **166**, 863 (1968).

²⁷U. Gerhardt and E. Mohler, *Phys. Status Solidi* **18**, K45 (1966).

²⁸A. A. Gavini and M. Cardona, *Phys. Letters* **27A**, 113 (1968).

²⁹T. Miyata and T. Tomiki, *J. Phys. Soc. Japan* **24**, 954 (1968); **24**, 954 (1968); **24**, 1408 (1968); **25**, 635 (1968); **27**, 658 (1969).

³⁰H. Saito, S. Saito, R. Onaka, and B. Ikeo, *J. Phys. Soc. Japan* **24**, 1095 (1968).

³¹H. Saito, S. Saito, and R. Onaka, *J. Phys. Soc. Japan* **27**, 126 (1969).

³²M. Watanabe, J. Nakamura, Y. Nakai, and T. Murata, *J. Phys. Soc. Japan* **26**, 1014 (1969).

³³H. Saito, M. Watanabe, A. Ejiri, S. Sato, H. Yamashita, T. Shibaguchi, H. Nishida, and S. Yamaguchi, *Solid State Commun.* **8**, 1861 (1970).

³⁴M. Watanabe and K. Nakamura, *J. Phys. Soc. Japan* (to be published).

³⁵H. R. Philipp and H. Ehrenreich, *Phys. Rev.* **131**, 2016 (1963).

³⁶D. M. Roessler and W. C. Walker, *Phys. Rev.* **166**, 599 (1968).

³⁷M. Watanabe, Y. Nakamura, Y. Nakai, and T. Murata, *J. Phys. Soc. Japan* **24**, 428 (1968).

³⁸D. Blechschmidt, R. Klucker, and M. Skibowski, *Phys. Status Solidi* **36**, 625 (1969).

³⁹G. Stephan and S. Robin, *Opt. Commun.* **1**, 40 (1969).

⁴⁰G. Stephan, E. Garignon, and S. Robin, *Compt. Rend.* **268**, 408 (1969).

⁴¹J. C. Lemonnier, G. Stephan, and S. Robin, *Compt. Rend.* **261**, 2463 (1965); *J. Opt. Soc. Am.* **57**, 486 (1967).

⁴²G. Stephan, Y. LeCalvez, J. C. Lemonnier, and S. Robin, *J. Phys. Chem. Solids* **30**, 601 (1969).

⁴³R. Haensel (private communication).

⁴⁴Other core bands (e.g., *s* states of the $-$ ions) occur in roughly the same energy range as the $+$ ion *p* states, but these additional core levels have small oscillator strengths for optical excitations to the lower-lying conduction bands and are therefore not important for the present discussion.

⁴⁵Although this model is the most widely accepted one, E. O. Steinborn and G. Gliemann [*Theoret. Chim. Acta* (Berlin) **4**, 185 (1966)] have interpreted the low-energy absorption bands in alkali halides in terms of one-electron excitations on the $-$ ions. According to this theory, the lowest-lying conduction bands are therefore associated with *d*-like states of the $-$ ions.

⁴⁶Thus the identification of the low-lying conduction bands with the excited states of the $+$ (rather than the $-$) ions is only approximate, but very useful for the analysis of chemical trends in the spectra. In most cases (see Refs. 7, 8, and 14) 70% or more of the charge density of these states is concentrated on the $+$ ion sites.

⁴⁷N. V. Starostin, *Fiz. Tverd. Tela* **11**, 1624 (1969) [*Sov. Phys. Solid State* **11**, 1317 (1969)].

⁴⁸L. Pincherle and P. M. Lee, *Proc. Phys. Soc. (London)* **78**, 1195 (1961).

⁴⁹G. Wannier, *Phys. Rev.* **52**, 191 (1937).

⁵⁰G. Dresselhaus, *J. Phys. Chem. Solids* **1**, 14 (1956).

⁵¹R. J. Elliott, *Phys. Rev.* **108**, 1384 (1957).

⁵²These effects can be directly incorporated into the exciton potential (1) using the dielectric function given by H. Haken, *Z. Naturforsch.* **9a**, 228 (1954); *Nuovo Cimento* **3**, 1230 (1956); *Fortschr. Physik* **6**, 271 (1958).

⁵³J. Frenkel, *Phys. Rev.* **37**, 17 (1931).

⁵⁴U. Gerhardt and G. W. Rubloff, *Appl. Opt.* **8**, 305 (1969).

⁵⁵Obtained from Harshaw Chemical Co.

⁵⁶Courtesy of Dr. S. Rice, The University of Chicago.

⁵⁷Obtained from Semi-Elements, Inc.

⁵⁸D. Blechschmidt, M. Skibowski, and W. Steinmann, *Phys. Status Solidi* **42**, 61 (1970).

⁵⁹Y. Iguchi, T. Sasaki, H. Sugawara, S. Saito, T. Nasu, A. Ejiri, S. Onari, K. Kojima, and T. Oya, *Phys. Rev. Letters* **26**, 82 (1971).

⁶⁰K. Siegbahn *et al.*, *ESCA Atomic, Molecular, and Solid State Structure Studied by Means of Electron Spectroscopy* (Almqvist and Wiksells, Uppsala, 1967), p. 72.

⁶¹T. Timusk and W. Martienssen, *Phys. Rev.* **128**, 1656 (1962).

⁶²J. A. Bearden and A. F. Burr, *Rev. Mod. Phys.* **39**, 128 (1967).

⁶³Y. Onodera and Y. Toyozawa, *J. Phys. Soc. Japan* **22**, 833 (1967).

⁶⁴L. Schultz, *Acta Cryst.* **4**, 487 (1951).

⁶⁵A. B. Kunz [*J. Phys. Chem. Solids* **31**, 265 (1970)] has shown that in RbI the conduction-band levels Γ_1 and X_3 should have negative and positive temperature shifts, respectively.

⁶⁶H. Saito *et al.* (Ref. 33) have given an alternative explanation of A_1^+ as a third component of an exciton triplet formed by the *p* hole and *d* electron in the atomic model.

⁶⁷P. Keil, *Z. Physik* **214**, 266 (1968).

⁶⁸However, such an analysis has been given for the Na^+ (*2p*) core excitons by S. Nakaj, T. Ishii, and T. Sagawa, *J. Phys. Soc. Japan* **30**, 428 (1971).

⁶⁹Y. Toyozawa, *Progr. Theoret. Phys. (Kyoto)* **20**, 53 (1958).

⁷⁰Recently we have found the spectra of CsI in region III to be similar to that of CsCl and CsBr.

⁷¹Differences in the absorption spectra of simple cubic (CsCl) and fcc (NaCl or rocksalt) phases of Cs halides have been observed previously: in the valence excitation region by A. A. Gavini and M. Cardona (Ref. 28) and in the soft x-ray region (corresponding to deep core level excitations) by M. Cardona, R. Haensel, D. W. Lynch, and B. Sonntag [*Phys. Rev. B* **2**, 1117 (1970)]. However, in these two crystal structures both the nearest-neighbor coordination of the $+$ ions and the shape of the Brillouin zone are different.

⁷²T. Sasaki, Y. Iguchi, H. Sugawara, S. Sato, T. Nasu, A. Ejiri, S. Onari, K. Kojima, and T. Oya, *J. Phys. Soc. Japan* **30**, 581 (1971).

- ⁷³D. Blechschmidt, M. Skibowski, and W. Steinmann, *Opt. Commun.* **1**, 275 (1970).
- ⁷⁴T. Sasaki, Y. Iguchi, H. Sugawara, S. Sato, T. Nasu, A. Ejiri, S. Onari, K. Kojima, and T. Oya, *J. Phys. Soc. Japan* **30**, 580 (1971).
- ⁷⁵H. Sugawara, T. Sasaki, Y. Iguchi, S. Sato, T. Nasu, A. Ejiri, S. Onari, K. Kojima, and T. Oya, *Opt. Commun.* **2**, 333 (1970).
- ⁷⁶R. Haensel, G. Keitel, G. Peters, P. Schreiber, B. Sonntag, and C. Kunz, *Phys. Rev. Letters* **23**, 530 (1969).
- ⁷⁷We assume here that the peaks are not simply a manifestation of structure in ϵ_2 (which might arise, e.g., from a dependence of the electron escape probability on the penetration depth of the light).
- ⁷⁸J. C. Phillips, in *Solid State Physics*, edited by H. Ehrenreich, F. Seitz, and B. Turnbull (Academic, New York, 1966), Vol. 18, p. 131.
- ⁷⁹U. Fano, *Phys. Rev.* **124**, 1866 (1961).
- ⁸⁰A classic example of this selection rule occurs in autoionization of the helium atom [see, e.g., E. U. Condon and G. H. Shortley, *The Theory of Atomic Spectra* (Cambridge U.P., New York, 1963), p. 371]. There, CI arises because of the Coulomb repulsion between the two electrons. This causes a discrete state of the atom to decay nonradiatively into a continuum state composed of a free electron and the He^+ ion. The process is described by the matrix element in (6) if the electron and hole states are replaced by the two electron states. The selection rule for the transition is then $\Delta J = \Delta P$ (parity) = $\Delta L = \Delta S = 0$.

⁸¹We assume that no other strong decay processes (be-

sides direct radiative, Auger, and Coulombic CI decay) are present.

- ⁸²F. C. Brown, C. Gähwiller, H. Fujita, A. B. Kunz, W. Scheifley, and N. Carrera, *Phys. Rev. B* **2**, 2126 (1970).
- ⁸³T. Sagawa, Y. Iguchi, M. Sasanuma, T. Nasu, S. Yamaguchi, S. Fujiwara, M. Nakamura, A. Ejiri, T. Masuoka, T. Sasaki, and T. Oshio, *J. Phys. Soc. Japan* **21**, 2587 (1966).
- ⁸⁴M. Cardona, R. Haensel, D. W. Lynch, and B. Sonntag, *Phys. Rev. B* **2**, 1117 (1970).
- ⁸⁵Y. Iguchi, T. Sagawa, S. Sato, M. Watanabe, H. Yamashita, A. Ejiri, M. Sasanuma, S. Nakai, M. Nakamura, S. Yamaguchi, Y. Nakai, and T. Oshio, *Solid State Commun.* **6**, 575 (1968).
- ⁸⁶S. Sato, T. Ishii, I. Nagakura, O. Aita, S. Nakai, M. Yokota, K. Ichikawa, G. Matsuoka, S. Kono, and T. Sagawa, *J. Phys. Soc. Japan* **20**, 459 (1970).
- ⁸⁷F. C. Brown, C. Gähwiller, A. B. Kunz, and N. O. Lipari, *Phys. Rev. Letters* **25**, 927 (1970).
- ⁸⁸N. O. Lipari and A. B. Kunz, *Phys. Rev. B* **3**, 491 (1971).
- ⁸⁹S. Nakai, T. Ishii, and T. Sagawa, *J. Phys. Soc. Japan* **30**, 428 (1971).
- ⁹⁰R. S. Bauer and W. E. Spicer, *Phys. Rev. Letters* **25**, 1283 (1970).
- ⁹¹M. Cardona, *Modulation Spectroscopy*, Suppl. II of *Solid State Physics*, edited by C. B. Duke (Academic, New York, 1969), pp. 150 and 284.
- ⁹²D. L. Camphausen, G. A. N. Connell, and W. Paul, *Phys. Rev. Letters* **26**, 184 (1971).

A Self-Consistent Procedure for the Linear-Combination-of-Atomic-Orbitals Method: Application to LiF^\dagger

D. M. Drost* and J. L. Fry‡

Department of Physics and Astronomy, Louisiana State University, Baton Rouge, Louisiana 70803

(Received 23 August 1971)

An efficient method for computing self-consistent energy bands within the framework of the linear-combination-of-atomic-orbitals (LCAO) method is applied to LiF . Efficiency of the method is a result of characteristically small LCAO secular determinants, the ease with which energy bands may be computed at general points in the Brillouin zone, and a formalism which expresses iterated-Hamiltonian matrix elements in terms of LCAO integrals computed in the first step only. A study of the self-consistent procedure is presented, including an investigation of convergence and accuracy. On the basis of this study it is concluded that self-consistent calculations using small Brillouin-zone samplings of symmetry points to compute charge densities contain errors as large as 1 eV. Accurate self-consistent energy bands are computed for LiF in the Hartree-Fock-Slater approximation and compared with previous calculations and experimental data. While an initial linear combination of ionic potentials with an adjustable exchange potential yields reasonable agreement with optical data, only a self-consistent potential produces agreement with both optical and photoemission data. It is suggested that to obtain reliable spectra, even when using an adjusted exchange potential, it is necessary to compute optical properties with self-consistent energy bands and wave functions.

I. INTRODUCTION

In the last five years there has been renewed interest in the linear-combination-of-atomic-orbitals

(LCAO) method for obtaining energy bands in solids. Although it is the oldest method of band calculation,¹ poor results from early inappropriate approximations caused it to fall into disfavor for a few decades.